Effect of Mistuning on Bending-Torsion Flutter using a Compressible Time-Domain Aerodynamic Theory

Senior Honors Thesis

Presented in Partial Fulfillment of the Requirements for Graduating with Distinction in the College of Engineering of The Ohio State University

By

Michael Patrick Thake, Jr.

Undergraduate Program in Aeronautical and Astronautical Engineering

The Ohio State University

2009

Senior Honors Thesis Committee:

Jack J. McNamara, Adviser

Jeffrey P. Bons

Abstract

The aircraft engine is a key element in improving overall performance of both military and civil aircraft. As designers look to improve performance, turbomachinery aeroelasticity, i.e. the study of fluid-structure interactions in compressors, is an important consideration when designing an efficient and reliable aircraft engine. Compressor designers are concerned with these interactions because there is a potential for structural failures due to flow-induced vibrations such as flutter. Flutter is a nearly instantaneous self-excited response that typically results in total structural failure. Because flutter poses as a sudden threat to aircraft safety, it is the center of this investigation. A method known as blade mistuning is tested to determine if it is a viable approach to reducing the occurrence of flutter. Mistuning is small deviations between blade stiffness and mass caused by manufacturing tolerances and wear. The effect of mistuned compressor blades on flutter has been studied over the past few decades and research has shown that a small amount of mistuning may have a beneficial effect on flutter velocity and could be used as a passive control method. The following investigation makes use of a recently developed unsteady aerodynamic model, based on the vortex lattice method, which is a discrete time-domain compressible flow solver applied to a two-dimensional, variable geometry cascade. The vortex lattice method is coupled with a typical section cascade structural

model to form a set of aeroelastic equations of motion. These equations of motion include the effects of mistuning by deviating pitching frequency. A Runge-Kutta integration scheme is implemented to solve the equations of motion. One method of calculating the flutter velocity and stability of a blade is by tracking damping. In this case, damping of the aeroelastic transient response is identified using a least-squares curve-fitting method. Damping of the response indicates system stability, where flutter is unstable, diverging oscillations. Results for this method are generated for two different cases. The first case is a twelve-blade cascade in a Mach 0.3 flow where alternate blade pitching frequency mistuning is studied with mistuning values of 0, 1, and 2%. Case two is a twenty-blade cascade in an incompressible flow where alternate blade pitching frequency mistuning is studied at values of 0, 1, 2 and 5% mistuning, as well as a case of random mistuning. The results show that mistuning introduces an exchange of energy between blades which improves the flutter velocity for a few blades in certain regions, but no drastic increase in flutter velocity was noted due to mistuning.

Dedication

Dedicated to my mother, Diane

Acknowledgements

I would like to thank my undergraduate research advisor, Professor Jack McNamara for all of his guidance and support through all of my research efforts. Without him, I would not have been encouraged to try or be successful in undergraduate research. I truly appreciate how Professor McNamara gave me my research topic and stepped back to let me take the reins. It was a challenge to do so much on my own, but it taught me a lot about research and solving problems. He has given me all the tools and confidence I need in all of my future endeavors. I would like to thank Professor Jeffrey Bons for being on this committee and helping me through the process. I cannot go without thanking the College of Engineering and the Engineering Honors Committee for funding me through the Undergraduate Research Scholarship. I would like to thank all of my friends, colleagues and family members for all of their support and assistance. I would like to thank Krista Kecskemety and Benjamin Szpak who helped me along the way with all the little things and worked with me to solve problems. I want to thank Julie Violand, who helped me revise my thesis and who has supported me every step of the way. She always listened and gave me the best advice and told me not to give up even when I thought I could not do it, thank you. Finally, I would like to thank my mother, Diane Thake, for being so supportive of me in everything I do. Without her, I would not be the person I am today, thank you.

Vita

2005……Dublin Scioto High School

2008 to Present……...Undergraduate Research Assistant, Department of Aerospace Engineering, The Ohio State University

2009 to Present……..University Fellow and Graduate Research Assistant, Department of Aerospace Engineering, The Ohio State University

2009……..Best Paper and Presentation Award, AIAA Region III Student Conference, University of Illinois

Fields of Study

Major Field: Aeronautical and Astronautical Engineering

Table of Contents

List of Tables

List of Figures

Nomenclature

A = coefficient matrix of vortex boundary conditions, $n+1$

a = elastic axis location, non-dimensional (positive aft); curve-fit coefficient; Dormand-Prince coefficient

B = number of blades; coefficient matrix of vortex boundary conditions, n

b = semi-chord length; curve-fit coefficient; Dormand-Prince coefficient

C = lift deficiency function; Whitehead force and moment coefficients

$C.G.$ = center of gravity

c = chord length; Dormand-Prince coefficient

e = elastic axis location from the mid-chord (positive aft)

F = aerodynamic force/moment vector

f = differential equation

H = Hankel function of the second kind

h = plunge displacement (positive down); Runge-Kutta time step

I_a = mass moment of inertia about elastic axis

K = kernel function; stiffness matrix

K_a = torsional stiffness

K_h = bending stiffness

k = blade index; reduced frequency, = $\omega b/U_\infty$

L = lift (positive up)

M = number of blade and wake vortex elements per blade; moment about the elastic axis (positive clockwise); mass matrix

M_∞ = freestream Mach number

m = blade mass

N = number of blade vortex elements per blade

q = state vector

r_a = blade radius of gyration

S_a = static mass moment of blade about elastic axis

s = number of stages

sc = blade spacing

t = time

U_∞ = freestream velocity

w = downwash velocity in the z direction

x = location of collocation point in the x direction

xo = location of vortex point in the x direction

x_a = static imbalance, non-dimensional (positive aft)

y = integrated Runge-Kutta vector

z = location of collocation point in the z direction

zo = location of vortex point in the z direction

α = pitch displacement/angle of attack in radians (positive clockwise)

β = weighting factor

Γ = strength of vortex elements (i.e. circulation)

Δx = blade element length

δ = percent mistuning

ζ = blade damping

θ = stagger angle

ρ = freestream air density

Σ = summation

ω_a = blade natural pitch frequency

ω_h = blade natural plunge frequency

Superscripts

k = blade index

l = blade index

n = time step index

-1 = matrix inverse

$\dot{}$ = first derivative, velocity

$\ddot{}$ = second derivative, acceleration

Subcripts

a = pitch

h = plunge

i = element or point index

j = element or point index

o = incompressible

1 = on the blade

2 = in the wake

Chapter 1: Introduction and Objectives

1.1 Introduction

Despite the significant evolution of the airplane from the Wright Flyer over the past century, global threats, tight profit margins and fluctuating fuel costs continually motivate the military and airline industry to seek improved aircraft performance and efficiency. The aircraft engine, shown in Fig. 1.1, plays an important role in defining many aspects of aircraft performance and efficiency, as the engine provides thrust, defines fuel efficiency and is an important factor in improving range and service ceiling. One method of improving performance and efficiency is by increasing the engine thrust-to-weight ratio.

The compressor is the section of the engine where an increase in thrust-to-weight ratio and overall performance can be realized. A computational mesh of a single compressor rotor is provided in Fig. 1.2. The purpose of the compressor is to use its blades to convert high velocity flow into high pressure flow for combustion and ultimately thrust. If the conversion can be performed with higher efficiency then a higher thrust can be achieved or less fuel will be required. This higher efficiency can be achieved by reducing the number of blades which reduces overall weight, but also requires that the blades have a higher blade loading. It is also important to reduce the

weight of a compressor by reducing blade weight, which often means a reduction in structural integrity. Thus, it is apparent that in order to optimize the compressor design, the compressor blades must carry a higher load and must be lighter, which is a compromise between aerodynamic efficiency, blade weight and structural integrity [1]. Looking at Fig. 1.3, it is evident that the structural engineer would like to increase efficiency by increasing the blade loading to blade weight ratio; however, a structural failures boundary is reached as that ratio becomes too large. It is the challenge of the structural engineer to push the structural failures boundary to the right so a higher efficiency can be realized, which requires an investigation of the interaction between the compressor fluid and structure.

1.2 Principles of Turbomachinery Aeroelasticity

The study of fluid-structure interactions, i.e. aeroelasticity [2], is complex because the study requires highly coupled structural-aerodynamic models which must be analyzed simultaneously. Collar's Expanded Triangle, shown in Fig. 1.4, shows all of the potential interactions within the field of aeroelasticity. This investigation is concerned with the aerodynamic, structural and inertial coupling.

The study of aeroelasticity in turbomachinery is further complicated due to the multifarious internal environment of turbomachinery. First, the compressor rotor is rotating which sets up an unsteady, periodic flowfield and produces inertial loads within

the blade structure. Second, the blades are typically thin and flexible. Third, the flow is highly unsteady due to the upstream disturbances (e.g. the fan and other compressor rotors) which produce wakes that affect the downstream blades. Finally, because the blades are tightly packed, there is very strong inter-blade interaction within a compressor causing aerodynamic coupling and further unsteadiness [1]. This dynamic and diverse environment has the potential to result in structural failures due to flow-induced vibrations such as flutter and high cycle fatigue.

High cycle fatigue, shown in Fig. 1.5, is a failure due to small amplitude oscillations that create cracks that propagate through the blade over time, which is a less catastrophic mode of failure and can be tested for during maintenance periods. Flutter is a nearly instantaneous self-excited response that typically results in total structural failure. Flutter is the result of overspeeding an engine causing rapidly diverging oscillations, shown in Fig. 1.6. Because flutter poses as a more immediate threat to aircraft safety, it will be the center of this investigation. It is critical that flutter is accurately and efficiently predicted and ultimately reduced to improve aircraft safety, performance and life expectancy, which is the objective of this investigation.

1.3 Literature Review

Flow-induced failures within compressors have been a major issue since the development of the gas turbine, as noted by reports of compressor and turbine vibration

problems as early as 1945 [3]. Even recently, there have been several documented cases of flutter during engine testing [4-9] due to the late emergence of research in turbomachinery aeroelasticity [1]. Engine designers have had great difficulty developing engines with flutter prevention with anything other than empirical models because there is a lack in understanding the fundamental principles of turbomachinery aeroelasticity as well as a lack in the development of a fast and accurate aeroelastic model. Because flutter is a matter of great concern, there has been a great deal of analytical, theoretical and computational research to discover more deeply the mechanisms that cause flutter as well as methods to actively or passively prevent flutter. The following literature review will cover the most significant research in turbomachinery aeroelasticity that will be applied to this thesis.

Two types of aeroelastic compressor models are studied. The first case studied is an ideal case in which all the compressor blades are assumed to be identical in structure, stiffness and mass. Fig. 1.7 shows the mode shapes of a tuned compressor rotor, which is the shape a blade will take under free vibration, an important consideration for aeroelastic studies. A tuned compressor rotor has mode shapes that are symmetric (i.e. cyclic symmetry) which allows for a simpler analysis because only one section of the compressor needs to be analyzed, saving computation time and model complexity.

Early flutter computation models, like the model developed by Bendiksen and Friedmann [10], use this simple tuned approach. Bendiksen and Friedmann use a two-dimensional typical section analysis with Whitehead's [11] unsteady cascade aerodynamics to locate the flutter boundary in the frequency-domain. Frequency-domain analyses, which means solving the set of differential equations of motion by converting them into algebraic equations through a Fourier Transform, was a common approach used in the early flutter computation models because it is simple and the use of differential equation solvers and computers are unnecessary. However, the frequency-domain approach also limits the problems that could be solved to simple harmonic motion problems. Fortunately, the flutter boundary exhibits simple harmonic motion as the blade transitions from converging to diverging oscillations. Thus, only the flutter boundary could be investigated, no actual blade motion or high cycle fatigue could be analyzed. Bendiksen and Friedmann discovered that coupling bending and torsion, and the use of structural damping, significantly affects the flutter boundary [10], and thus the aeroelastic equations of motion should always include two degrees of freedom (i.e. bending and torsion) for an accurate representation of the system.

Cho et al. [12] performed a more recent time-domain analysis using a three-dimensional unsteady vortex lattice method to model the unsteady aerodynamics. The time-domain analysis allows any blade motion to be analyzed, not just simple harmonic motion. With this new analysis method, Cho et al. concluded an important point about

the relationship between the number of blades, aerodynamics and system stability. Cho found that increasing the number of blades increases flow unsteadiness which destabilizes the aeroelastic system and leads to a decrease in flutter speed. This conclusion shows that turbomachines are at a strong aeroelastic disadvantage because of the large number of blades. It is crucial that flutter within turbomachines be further investigated.

The tuned compressor analyses are insightful but do not look deep into the mechanisms that cause flutter because those analysis methods assume a simple model and do not take into account real effects. In reality, compressor blades, although they are intended to be identical, have small deviations from each other (i.e. mistuning), caused by manufacturing tolerances and wear. Mistuning sets up localized mode shapes, as seen in Fig. 1.8, at much higher amplitudes than those of the tuned case which destroys the assumption of cyclic symmetry. Because the compressors' mode shapes are no longer symmetric, the entire system must be analyzed posing a difficult and lengthy computation problem.

The effect of mistuning on flutter was not investigated until the 1960's and 1970's, a decade after researchers began studying tuned turbomachinery flutter. Movshovich [13], Dye and Henry [14], Ewins [15,16], and Whitehead [17-19] were among the first to study mistuning and arrive at conclusions on the effect of mistuning on

flutter in turbomachines. Because they each derived different models and made different assumptions about inter-blade phase angle, they arrived at different conclusions. Some aeroelasticians concluded that mistuning was never beneficial to flutter, while others argued that mistuning was always beneficial to flutter stability. However, they all agreed that mistuning may have an adverse affect on forced response but can be eliminated with elegant mistuning arrangements.

Kaza and Kielb [20] performed a more rigorous frequency-domain investigation on the effect of mistuning on a two-dimensional blade row using a model similar to Ref. 10 and concluded that a small amount of mistuning can have a beneficial effect on flutter velocity and can be used as a passive control method.

A more recent time-domain flutter analysis using a mistuned turbine was performed by Sadeghi and Lui [21]. They used alternate frequency mistuning, where the natural frequency of neighboring blades alternates between a high and low value, which they confirmed may have a stabilizing effect on flutter. It was found that mistuning averaged the stable and unstable blade modes by changing the inter-blade phase angle. Sadeghi and Lui also found that increasing the level of mistuning decreases the maximum amplitude of the blades, a benefit to not only flutter but also high cycle fatigue. A final discovery of Sadeghi and Lui was that the mass ratio has a significant effect on the minimum mistuning level to stabilize a system.

1.4 Objectives

The objective of the research presented in this thesis is to verify previous findings and investigate the effects of mistuning on a compressor to determine if it is a viable approach to passively reduce the occurrence of flutter. A fast and accurate unsteady aerodynamic model will be developed for a cascade in the time-domain which will be coupled with a mistuned structural model to create a set of aeroelastic equations of motion. A study will be performed on the aerodynamic model to determine its usability as an accurate unsteady aerodynamic model. The equations of motion will be solved using a differential equation solver to compute the transient response of each blade. System damping will be extracted from the transient response using a system identification tool. Then using the system damping, the system stability and flutter boundary can be located. Mistuning and stability trends will be analyzed to determine the practicality of using mistuning as an approach to reducing flutter.

Chapter 2: Formulation of the Problem

2.1 Compressor Model Reduction

One key assumption made throughout this study is in the modeling of the compressor. The three-dimensional compressor, shown in Fig. 1.2, is reduced to a two-dimensional cascade which is a typical reduction as noted in Ref. 1. Figure 2.1 shows the cascade which linearizes the compressor by cutting and unraveling it so it becomes two-dimensional. As seen in Fig. 2.1, the cascade is easy to define because it only requires three parameters: chord length, stagger angle and blade spacing. This reduction allows for significantly faster computation and lower cost while still producing the same general trends.

2.2 Unsteady Aerodynamic Model

The unsteady aerodynamic model selected for this analysis is a vortex lattice method (VLM) applied to a cascade – an approach that provides a good balance between flexibility, computational efficiency and accuracy. Benefits of the vortex lattice method over many other unsteady aerodynamic models are the flexibility to account for flow compressibility, viscosity, blade camber and thickness, the ability to accurately model the wake, and the capacity to provide lift and moment in the time domain given any input.

The vortex lattice method can be used in two-dimensional or three-dimensional flow with either a single airfoil or a cascade of any number of airfoils with any cascade geometry.

An appropriate vortex lattice method aerodynamic model has been developed in Ref. 22 for a single isolated airfoil, which along with Ref. 23, is the basis of the model developed for this thesis. The model in Ref. 22 is applied to a 2-D cascade of airfoils with a set stagger angle, blade spacing and number of blades, and is adapted to include compressibility. The model assumes that the incoming flow is inviscid and irrotational. It also neglects the effects of an engine casing, shrouds, upstream disturbances such as other blade rows, and three-dimensional effects. For simplicity, the model is a single isolated blade row strung out into a cascade.

The fundamental concept behind the unsteady vortex lattice method is to replace each airfoil with a specified number of blade and wake vortex (i.e. circulation) elements, illustrated in Fig. 2.2, to simulate the bound circulation on the blade and the free circulation shed behind the airfoil. The blade element vortex strength is used to calculate lift and moment. The wake element is used to conserve vorticity which inherently creates unsteadiness because the wake is constantly moving and/or changing strength. Figure 2.3 gives a visualization of the vortex lattice method used on a cascade of blades where the red elements are the blade element vortex points and the blue elements are the wake element vortex points.

For each blade element, the vortex strength, Γ, is bound at the vortex point (the element ¼-chord). These vortex elements are created from the downwash velocity from the blade motion at the collocation point (the element ¾-chord point), shown in Fig. 2.2, which is given in Eq. (1) [22],

$$\begin{Bmatrix} {}^{k}\Gamma_1^n \\ {}^{k}\Gamma_2^n \end{Bmatrix} = \begin{bmatrix} {}^{k}K_1 & {}^{k}K_2 \end{bmatrix}^{-1} {}^{k}w^n \tag{1}$$

where K is the Kernel function for a infinite 2-D vortex filament [23], defined in Eq. (2) and Eq. (3),

$$ {}^{k,l}K_1 = \frac{{}^{k}x_i - {}^{l}xo_j}{2\pi\left(\left({}^{k}x_i - {}^{l}xo_j\right)^2 + \left({}^{k}z_i - {}^{l}zo_j\right)^2\right)} \tag{2}$$

$$for\ i = 1 \dots N, j = 1 \dots N, k = 1 \dots B, l = 1 \dots B$$

$$ {}^{k,l}K_2 = \frac{{}^{k}x_i - {}^{l}xo_j}{2\pi\left(\left({}^{k}x_i - {}^{l}xo_j\right)^2 + \left({}^{k}z_i - {}^{l}zo_j\right)^2\right)} \quad (3) $$

$$ for\ i = 1 \dots N, j = N+1 \dots M, k = 1 \dots B, l = 1 \dots B $$

where N is the number of blade elements, M is the number of blade and wake elements, k is the blade index, n is the time step, Γ is the vortex strength and the subscript *1* and *2* denote the blade and wake, respectively.

The downwash velocity, w, is given in Eq. (4), which is the sum of the velocity components normal to the blade caused by an angle of attack into the freestream velocity, as well as plunge velocity and pitch velocity. It is important to note that because the blade movement is assumed to be small, it permits the use of the small angle approximation, allowing for a less complex equation that is still accurate.

$$ {}^{k}w = U_\infty \tan\alpha + \dot{h} + (x - 2\,\mathrm{b}\,\mathrm{sc}\,(k-1)\tan\theta)\,\dot{\alpha}\,sec^2\alpha \quad (4) $$

In the wake, a vortex is shed from the trailing edge of the blade at each time step. The strength of the wake vortex element shed from the trailing edge, defined in Eq. (5),

satisfies conservation of vorticity. Essentially, the sum of circulation created on the blade due to lift at that time step is negated by the first shed vortex to ensure no circulation is created in the overall system. The strength of the following wake vortices is convective, as noted in Eq. (6). Thus for this model, the wake elements stay motionless in the streamwise direction, but the strength of each vortex moves to the next wake element at every time step. That is, each i^{th} wake vortex element will have the strength of the i^{th}-*1* wake vortex element at the next time step. The theoretically infinitely long wake is approximated as a wake of finite length by the use of a weighting factor, β, on the final wake element, as in Eq. (7). It has been suggested by Hall [24] to use a weighting factor of between 0.95 and 1 to accurately cut off the wake.

$$ {}^{k}_{N+1}\Gamma_2^{n+1} = -\sum_{i=1}^{N}\left({}^{k}_{i}\Gamma_1^{n+1} - {}^{k}_{i}\Gamma_1^{n}\right) \tag{5} $$

$$ {}^{k}_{i}\Gamma_2^{n+1} = {}_{i-1}{}^{k}\Gamma_2^{n} \quad (i = N+2 \ldots M-1) \tag{6} $$

$$ {}^{k}_{M}\Gamma_2^{n+1} = \beta\, {}^{k}_{M}\Gamma_2^{n} + {}_{M-1}{}^{k}\Gamma_2^{n} \tag{7} $$

The wake convection, conservation and cut off boundary conditions are condensed into the matrices A and B in Eq. (8), which satisfy Eq. (5), Eq. (6) and Eq. (7).

$$\begin{bmatrix} {}^{k}A_1 & {}^{k}A_2 \end{bmatrix} \begin{Bmatrix} {}^{k}\Gamma_1 \\ {}^{k}\Gamma_2 \end{Bmatrix}^{n+1} = \begin{bmatrix} {}^{k}B_1 & {}^{k}B_2 \end{bmatrix} \begin{Bmatrix} {}^{k}\Gamma_1 \\ {}^{k}\Gamma_2 \end{Bmatrix}^{n} \tag{8}$$

The matrices A and B are defined in Eq. (9) through (12) as,

$${}^{k}A_1 = \begin{bmatrix} 1 & \cdots & \cdots & \cdots & 1 \\ 0 & \cdots & \cdots & \cdots & 0 \\ \vdots & \ddots & \ddots & \ddots & \vdots \\ \vdots & \ddots & \ddots & \ddots & \vdots \\ 0 & \cdots & \cdots & \cdots & 0 \end{bmatrix} \quad (M - N \; x \; N) \tag{9}$$

$${}^{k}A_2 = \begin{bmatrix} 1 & 0 & 0 & 0 & 0 \\ 0 & \ddots & 0 & 0 & 0 \\ 0 & 0 & 1 & 0 & 0 \\ 0 & 0 & 0 & \ddots & 0 \\ 0 & 0 & 0 & 0 & 1 \end{bmatrix} \quad (M - N \; x \; M - N) \tag{10}$$

$$ {}^{k}B_1 = \begin{bmatrix} 1 & \cdots & 1 & \cdots & 1 \\ 0 & \cdots & \cdots & \cdots & 0 \\ \vdots & \ddots & \ddots & \ddots & \vdots \\ \vdots & \ddots & \ddots & \ddots & \vdots \\ 0 & \cdots & \cdots & \cdots & 0 \end{bmatrix} \quad (M - N \; x \; N) \tag{11} $$

$$ {}^{k}B_2 = \begin{bmatrix} 0 & 0 & 0 & 0 & 0 \\ 1 & \ddots & 0 & 0 & 0 \\ 0 & \ddots & \ddots & 0 & 0 \\ 0 & 0 & \ddots & 0 & 0 \\ 0 & 0 & 0 & 1 & \beta \end{bmatrix} \quad (M - N \; x \; M - N) \tag{12} $$

The previous equations are organized and compacted for efficient computing of multiple blade aerodynamics, which follow Eq. (13), (14) and (15).

$$ A_{1,2} = \begin{bmatrix} {}^{1}A_{1,2} & 0 & 0 & 0 & 0 \\ 0 & \ddots & 0 & 0 & 0 \\ 0 & 0 & {}^{k}A_{1,2} & 0 & 0 \\ 0 & 0 & 0 & \ddots & 0 \\ 0 & 0 & 0 & 0 & {}^{B}A_{1,2} \end{bmatrix} \tag{13} $$

$$K_{1,2} = \begin{bmatrix} {}^{1,1}K_{1,2} & \cdots & {}^{1,l}K_{1,2} & \cdots & {}^{1,B}K_{1,2} \\ \vdots & \ddots & \ddots & \ddots & \vdots \\ {}^{k,1}K_{1,2} & \ddots & {}^{k,l}K_{1,2} & \ddots & {}^{k,B}K_{1,2} \\ \vdots & \ddots & \ddots & \ddots & \vdots \\ {}^{B,1}K_{1,2} & \cdots & {}^{B,l}K_{1,2} & \cdots & {}^{B,B}K_{1,2} \end{bmatrix} \tag{14}$$

$$w^n = \begin{bmatrix} {}^{1}w^n \\ \vdots \\ {}^{k}w^n \\ \vdots \\ {}^{B}w^n \end{bmatrix} \tag{15}$$

The wake vortex strength is calculated in Eq. (16) using static condensation [25] and combining Eq. (1) and Eq. (8).

$$\begin{aligned} \Gamma_2^n = (-A_1K_1^{-1}K_2 + A_2)^{-1}[(-B_1K_1^{-1}K_2 + B_2)\Gamma_2^{n-1} - A_1K_1^{-1}w^n \\ + B_1K_1^{-1}w^{n-1}] \end{aligned} \tag{16}$$

By providing the downwash velocity, from Eq. (4), at each blade element and solving Eq. (16) for the wake vortex strength, the final aerodynamic equation, Eq. (17), is solved which gives the blade vortex element strength at each time step.

$$\Gamma_1^n = -K_1^{-1}K_2^n\Gamma_2^n + K_1^{-1}w^n \tag{17}$$

Unsteady incompressible lift and moment for each blade is calculated about the elastic axis using the blade vortex element strength from Eq. (17) [24]. Equations (18) and (19) are the discretized Kutta-Joukowsky equations used to calculate lift and moment at the elastic axis [22].

$${}^kL_0^n = \rho U_\infty \sum_{i=1}^{N} {}_i^k\Gamma_1^n \tag{18}$$

$${}^kM_0^n = \rho U_\infty \sum_{i=1}^{N} \left({}^kxo_i - e \right) {}_i^k\Gamma_1^n \tag{19}$$

The effect of low speed compressibility is incorporated using the Prandtl-Glauert rule [26], which is approximated in Eq. (20) and Eq. (21). The Prandtl-Glauert correction is only accurate for flows less than Mach 0.6, which is satisfied in this analysis.

$$ {}^{k}L^{n} = \frac{{}^{k}L_{0}^{n}}{\sqrt{1 - M_{\infty}^{2}}} \tag{20} $$

$$ {}^{k}M^{n} = \frac{{}^{k}M_{0}^{n}}{\sqrt{1 - M_{\infty}^{2}}} \tag{21} $$

2.3 Mistuned Structural Model

For the structural model, the blade is modeled as a typical section. A typical section is a 2-D cross-section of an airfoil taken at the 70-75% span location, which accurately represents the full blade characteristics in two dimensions [27]. The typical section used in this model is shown in Fig. 2.4. The structural dynamics of the blades are modeled using a simple two degree-of-freedom (plunge and pitch) spring system. The bending (plunge degree of freedom) and torsional (pitch degree of freedom) elastic

stiffness of the blades are replaced using translational and torsional springs, with the inertial effects included in the stiffness of these springs.

The point at which the elastic-inertial forces are located is the elastic axis, e. The aerodynamic forces are located at the aerodynamic center; however they are shifted to the elastic axis for this analysis. Static imbalance, x_a, is the offset between the center of gravity and elastic axis. The static imbalance is an important parameter because it provides a method of blade mode coupling. The blade surface itself, representing the aerodynamic shape, is assumed to be flat and rigid. Small blade deflections are assumed so that small angle approximation can be employed.

To include alternate blade mistuning, a key element to the analysis, the natural pitching frequency is alternately increased and decreased for adjacent blades by half of the overall mistuning value. As an example, for 1% mistuning, all even blade pitching frequencies would be multiplied by 1.005 and all odd blade pitching frequencies would be multiplied by 0.995. This allows the entire cascade to remain balanced and maintain the same average natural pitching frequency. Although this type of mistuning does not represent the actual variations of blades, it still provides the general trends of mistuning. A more realistic method of blade mistuning is random mistuning, where the natural pitching frequency is randomly changed from blade to blade.

2.4 Aeroelastic Model

The aeroelastic equations of motion combine the unsteady aerodynamic model and the mistuned structural model to obtain a coupled system of equations, shown in Eq. (22). The equations of motion are derived using Lagrange's equation along with kinetic and strain energy.

$$M\ddot{q} + Kq = F \tag{22}$$

M and K are the mass and stiffness matrices from the mistuned structural model, defined in Eq. (23) and Eq. (24). q is the state vector, which contains the pitch, plunge, velocity and acceleration of each blade, and F is the force/moment matrix from the unsteady aerodynamic model, defined in Eq. (25).

$$M = \begin{bmatrix} m & S_a \\ S_a & I_a \end{bmatrix} \tag{23}$$

$$K = \begin{bmatrix} K_h & 0 \\ 0 & {}^{k}K_a \end{bmatrix} \tag{24}$$

$$F = \begin{bmatrix} -L \\ M \end{bmatrix} \tag{25}$$

S_a, I_a, K_h and K_a are defined in Eq. (26).

$$\begin{aligned} S_a &= mbx_a & I_a &= mr_a^2 \\ K_h &= m\omega_h^2 & {}^{k}K_a &= I_a^k \omega_a^2 \end{aligned} \tag{26}$$

It is important to note that Eq. (22) is calculated separately for each blade. The only coupling terms between the blades of the cascade are the aerodynamic lift and moment, L and M.

Blade mistuning becomes inherent in the pitch natural frequency, which is calculated in Eq. (27).

$$^{k}\omega_a = \omega_a\left(1 \pm {}^{k}\delta\right) \tag{27}$$

2.5 System Integration and Identification

A fast and accurate integration scheme is used to solve the aeroelastic equations of motion. An explicit Runge-Kutta 4-5th order scheme, also referred to as the Dormand-Prince pair [28], is implemented as the solver. It is called a 4-5th order because the integration scheme selects the order of accuracy based on its position in the differential equation. The general Runge-Kutta integration scheme is given in Eq. (28),

$$\begin{aligned} g_i &= y_n + h\sum_{j=1}^{s} a_{i,j}k_j \\ k_i &= f(t_n + c_i h, g_i) \quad (i = 1,2,\dots,s) \\ y_{n+1} &= y_n + h\sum_{i=1}^{s} b_i k_i \end{aligned} \tag{28}$$

where y is the actual position, or state vector in this case, f is the differential equation, s is the number of stages, h is the time step and a, b, and c are the Dormand-Prince

coefficients defined in Table 2.1 [28]. Within Table 2.1, each row is a stage, the blue section corresponds to the *a* coefficients, the red section corresponds to the *b* coefficients where the first row provides the fourth-order accurate solution and the second row provides the fifth-order accurate solution, and the yellow section corresponds to the *c* coefficients.

This integration scheme is a one-step solver, meaning it only requires the previous time step to calculate the next time step. The code is an adaptive time-step, non-stiff solver which allows it to pass through the range of time steps quickly while maintaining a medium amount of accuracy. Although this is an adaptive time-step solver, it has been forced to have a constant time-step as required by the wake model.

The solution to the equations of motion provides the blade response for any given input. One method of calculating the flutter velocity and stability of a blade is by tracking system response damping. Positive damping means the blades are converging to their steady state position, meaning they are stable. Zero damping indicates neutral oscillations because the oscillations are neither converging nor diverging. The zero damping line is referred to as the flutter boundary because any less damping is unstable. Negative damping indicates oscillations that are diverging from the steady state position (i.e. flutter). In this case, damping of the aeroelastic transient response is identified using a least-squares curve-fitting method. The least squares-curve fit, used by McNamara and Friedmann [29], uses a combined exponential and harmonic function to fit the transient

response, shown in Eq. (29) and Eq. (30). The transient response is fit by guessing variables in Eq. (29) and (30) until the error requirement is met.

$$h(t) = a_0 + e^{-\zeta_h \omega_h t}\{a_h \cos(\omega_h^2(1-\zeta_h)t) + b_h \sin(\omega_h^2(1-\zeta_h)t)\} \tag{29}$$

$$\alpha(t) = a_0 + e^{-\zeta_a \omega_a t}\{a_a \cos(\omega_a^2(1-\zeta_a)t) + b_a \sin(\omega_a^2(1-\zeta_a)t)\} \tag{30}$$

Chapter 3: Results

3.1 Unsteady Aerodynamics

The vortex lattice method presented in this paper is compared against several other simpler aerodynamic models to examine the accuracy of the vortex lattice method and to view the differences between each theory. Three single blade aerodynamic theories are used for comparison: quasi-static, quasi-steady and Theodorsen's [27]. One cascade aerodynamic theory, Whitehead's [11], is used.

Quasi-static aerodynamics is the simplest aerodynamic theory available because it does not account for inertial forces, phase lag, aerodynamic damping, or lift deficiency due to the wake. However, the benefit of this imprecise theory is that it can be used for arbitrary blade motion, not just prescribed simple harmonic motion. Equation (31) and (32) give the lift and moment as calculated by quasi-static aerodynamics. The lift and moment are calculated about the aerodynamic center which is shifted to the elastic axis as required by the aeroelastic model.

$$L = 2\pi\rho U_\infty b\left[\dot{h} + U_\infty \alpha\right] \tag{31}$$

$$M = -L[ba + (b/2)] \tag{32}$$

Quasi-steady aerodynamics is a more sophisticated theory which includes aerodynamic damping and inertial forces. It can also be applied to arbitrary motion. Although quasi-steady aerodynamics is better than quasi-static, it still does not account for phase lag and lift deficiency due to the wake, important effects in the study of turbomachinery aerodynamics. The equations for quasi-steady aerodynamics can be found in Eq. (33) and (34).

$$L = \pi\rho b^2\left[\ddot{h} + U_\infty\dot{\alpha} - ba\ddot{\alpha}\right] + 2\pi\rho U_\infty b\left[\dot{h} + U_\infty\alpha + b\left(\frac{1}{2} - a\right)\dot{\alpha}\right] \tag{33}$$

$$\begin{aligned} M = \pi\rho b^2 &\left[ba\ddot{h} - U_\infty b\left(\frac{1}{2} - a\right)\dot{\alpha} - b^2\left(\frac{1}{8} - a^2\right)\ddot{\alpha}\right] \\ &+ 2\pi\rho U_\infty b^2\left(a + \frac{1}{2}\right)\left[\dot{h} + U_\infty\alpha + b\left(\frac{1}{2} - a\right)\dot{\alpha}\right] \end{aligned} \tag{34}$$

Theodorsen's aerodynamic theory includes the effect of the wake, which is built in to the *C(k)* coefficient, or the lift deficiency function. This lift deficiency function, which is defined in Eq. (35) where *H* is the Hankel function of the second kind and *k* is the reduced frequency, reduces the magnitude of lift and produces a phase lag. However, a downside to the use of this deficiency function is that it assumes simple harmonic motion which limits the range of problems to be solved to be only forced motion or the flutter boundary, where the motion is exactly simple harmonic. Comparing Eq. (36) and (37), which are the equations for lift and moment of Theodorsen's unsteady aerodynamics, to the quasi-steady equations it is seen that the equations are nearly identical other than the inclusion of the lift deficiency function in the second term of both lift and moment in Theodorsen's aerodynamics.

$$C(k) = \frac{H_1^{(2)}(k)}{H_1^{(2)}(k) + iH_0^{(2)}(k)} \tag{35}$$

$$L = \pi\rho b^2\left[\ddot{h} + U_\infty\dot{\alpha} - ba\ddot{\alpha}\right] + 2\pi\rho U_\infty bC(k)\left[\dot{h} + U_\infty\alpha + b\left(\frac{1}{2} - a\right)\dot{\alpha}\right] \tag{36}$$

$$M = \pi\rho b^2 \left[ba\ddot{h} - U_\infty b\left(\frac{1}{2} - a\right)\dot{\alpha} - b^2\left(\frac{1}{8} - a^2\right)\ddot{\alpha} \right] + 2\pi\rho U_\infty b^2 C(k)\left(a + \frac{1}{2}\right)\left[\dot{h} + U_\infty \alpha + b\left(\frac{1}{2} - a\right)\dot{\alpha}\right] \quad (37)$$

The vortex lattice method is compared to these single blade aerodynamic theories under both high (k = 0.3) and low (k = 0.01) unsteadiness values in prescribed simple harmonic motion. Figure 3.1 shows the results generated for a single blade under a flow with low unsteadiness. Because there is a low amount of unsteadiness, all three theories agree, as shown in Fig. 3.1.

It is also expected that at high values of unsteadiness, the theories diverge in accordance with the robustness of their aerodynamic modeling. Figure 3.2 shows the relationship between each theory under a highly unsteady flow. It can be seen that because the vortex lattice method and Theodorsen's theory both include unsteadiness, the magnitude of their lift is far reduced from that predicted by the quasi-static and quasi-steady models which do not account for flow unsteadiness by neglecting wake effects. It can also be seen that the vortex lattice method and Theodorsen's theory match up very well. As Fig. 3.2 is looked at closer, it can be seen that as unsteadiness is included by the lift deficiency coefficient to the quasi-steady case, a phase lag is introduced into Theodorsen's and the vortex lattice method prediction.

From this single blade aerodynamic comparison, Theodorsen's prediction that unsteadiness introduces a reduction in lift magnitude and creates a phase lag is computationally confirmed. This vortex lattice model is also determined to be accurate for the single blade case. To more accurately confirm the vortex lattice method in a highly unsteady flow, it should be compared to a high fidelity computational fluid dynamics model.

Next, Whitehead's theory and the vortex lattice method are evaluated in a cascade. Whitehead's theory is the simplest cascade aerodynamic theory available. It assumes an infinite cascade, uses a vortex sheet method, and accounts for lift deficiency from the wake. The downside is that it assumes simple harmonic motion, so arbitrary motion cannot be analyzed. Whitehead's theory is basically Theodorsen's theory applied to a cascade. It has been proven that if Whitehead's theory assumed infinite blade spacing, the solution would converge to Theodorsen's single blade aerodynamics [11]. The equations to obtain Whitehead's unsteady lift and moment about the leading edge can be found in Eq. (38) and (39). The coefficients C_{Fq}, $C_{F\alpha}$, C_{Mq}, and $C_{M\alpha}$ have been calculated by Whitehead [11].

$$L = 2\pi\rho Ub\left(\dot{h}C_{Fq} + \alpha U C_{F\alpha}\right) \tag{38}$$

$$M = 4\pi\rho U b^2\left(\dot{h}C_{Mq} + \alpha U C_{M\alpha}\right) \tag{39}$$

Although Whitehead's theory assumes an infinite cascade which is impossible to analyze for the vortex lattice method, the theories can be compared by examining the trend as more blades are added to the cascade for the vortex lattice method. Figure 3.3 shows Whitehead's theory compared to the vortex lattice method for one blade, five blades and ten blades at a moderate unsteadiness value (k = 0.1). The figure shows that the single blade produces the most lift. It is seen that as blades are added to the cascade, they produce more unsteadiness because there is wake-to-blade interaction which reduces the lift, as predicted. A larger reduction in lift is noticed when blades are added to a smaller cascade (i.e. one to five blades) because each blade added significantly increases the overall circulation and unsteadiness which causes the few blades to be severely impacted. However as more blades are added (i.e. five to ten blades), the effect becomes less apparent because the addition of each blade is a small portion of the overall system.

Two important trends can be noted from Fig. 3.3. First, as the number of blades in the vortex lattice method cascade increases, the solution moves toward the magnitude of Whitehead's prediction. Second, the vortex lattice method, because it has a better unsteadiness model, has a larger phase lag than what Whitehead predicted. On a similar note, it is interesting that the phase lag does not increase as the number of blades

increase, the cause of which is either because only the center blade is looked at or the blade motion for the aerodynamic testing is forced and not free. It can be concluded from Fig. 3.3 that the vortex lattice method applied to a cascade agrees well with Whitehead's theory and becomes very accurate when more than ten blades are added to the cascade.

3.2 Tuned Cascade

Before mistuning is investigated, the trends of a tuned cascade must first be analyzed which will performed for two separate cases. The first case is a twelve-blade cascade in a Mach 0.3 flow, where all the blades are simultaneously disturbed. The disturbance is a small velocity given to both pitch and plunge. The remaining blade and flow properties are found in Table 3.1. Only twelve blades are analyzed because it is computationally inexpensive and still provides the general trends, although it is not representative of a full compressor. Case two is a twenty-blade cascade in an incompressible flow, where only the middle blade is disturbed with a pitch and plunge velocity. Table 3.2 gives the parameters used for the flow, cascade structure and blade properties for case two.

The results for the case one tuned cascade are provided in Fig. 3.4 and Fig. 3.5 which give the damping for all twelve individual blades, each represented by a curve. As seen from Fig. 3.4, the cascade is stable in plunge for every calculated freestream velocity and becomes more stable as the freestream velocity is increased. However for

pitch stability, shown in Fig. 3.5, all of the blades except one remain stable as freestream velocity is increased. The single unstable blade begins to flutter around 53 ft/s, which causes the system to fail because the diverging oscillations become too large.

Case two results for a tuned cascade can be observed in Fig. 3.6 and Fig. 3.7. Here, only the damping values of the middle 14 blades of the cascade are shown to provide a clearer picture of stability. Plunge stability, given in Fig. 3.6, shows a similar trend as Fig. 3.4 in that as freestream velocity increases, the damping increases. However, the overall system is highly unstable because all of the blade damping values, except one, have negative values. The single stable blade is the middle blade, which was the blade that was disturbed. From Fig. 3.6, it is concluded that as the center blade is disturbed is creates an unsteady wake which effects the remaining blades in the cascade and causes them to become unstable. This phenomenon allows the middle blade to remain stable. The pitch stability from Fig. 3.7, starts unstable but stabilizes around 63 ft/s. The middle blade appears to be the most stable for the same reasons observed in Fig. 3.6.

3.3 Mistuned Cascade

The ultimate goal in this study is to utilize a variety of mistuning methods to stabilize the blade system sooner and/or prevent flutter from occurring. In the first case, alternate blade pitching frequency mistuning is studied with mistuning values of 1 and

2%. In the second case, alternate blade pitching frequency mistuning is also studied at values of 1, 2 and 5% mistuning, as well as a case of random mistuning. The values used for the random mistuning are given in Table 3.3 which are randomly generated values within about 10% mistuning. The same properties in Table 3.1 (case one) and Table 3.2 (case two) are used to evaluate mistuning.

For case one, the result of 1% mistuning is shown in Fig. 3.8 and Fig. 3.9. Plunge stability remains essentially unchanged with the exception of a few blades becoming more or less stable indicating that some blades are losing energy and others are gaining energy. Thus, mistuning sets up an exchange of energy between the blades which could potentially lead to a reduction in flutter if the correct blades are mistuned. On another note, the pitch stability goes through some considerable changes as mistuning is added. The same trend is observed where certain blades become less stable because they are extracting more energy from both the flow and the other blades. However, the result is that blades begin fluttering well before the tuned case flutter velocity of 53 ft/s. This effect is highly undesirable and contradicts Whitehead's proposal that small amounts of mistuning is beneficial.

To determine if mistuning is still a viable approach to reducing the occurrence of flutter in case one, 2% mistuning is analyzed to ensure further mistuning would not eventually stabilize the cascade. Examining Fig. 3.10 and Fig. 3.11, more mistuning only appears to exacerbate the problem. More blades begin to flutter at lower freestream

velocities. The blades also have more negative damping values than the 1% case, meaning the amplitude of blade oscillations is growing faster.

Although case one concludes that mistuning is not beneficial for stability, a second case is tested to confirm, oppose or limit the results. The results of 1% mistuning for case two are given in Fig. 3.12 and Fig. 3.13. A few blades in the plunge degree of freedom become a lot more stable; however this comes at the cost of causing most of the other blades to become slightly less stable. The center blade is unaffected by this small amount of tuning. Overall the plunge degree of freedom remains unstable. In the pitch degree of freedom, the addition of mistuning causes the system to become more unstable at freestream velocities below 40 ft/s, however, the system stability increases when the freestream velocity is above 40 ft/s. With this, mistuning is successful in preventing the occurrence of flutter at a particular velocity in one of the degree of freedoms. Although the plunge degree of freedom remains unstable, this is a large leap towards the successful use of mistuning.

Mistuning will be further analyzed by increasing the mistuning value to 2%. Figures 3.14 and 3.15 give the plunge and pitch stability results for this case. Plunge stability improves slightly with the increase in mistuning, but not enough to make a difference because it is still overall unstable. Pitch stability loses its mistuning benefits around 40-60 ft/s from the increase of mistuning, but it is still better than the tuned

cascade. These results conclude that the maximum benefit of mistuning might occur around 1% mistuning.

For completeness, 5% mistuning was investigated for case two. The results are provided in Fig. 3.16 and Fig. 3.17. The effect of the increase in mistuning changes the plunge stability by reducing the damping of certain blades while improving the damping of others, a trend noticed earlier. Overall, the plunge stability does not appear to benefit from the increase in mistuning. The pitch stability, conversely, sees major benefits from the increase in mistuning. The overall stability in pitch is better for almost all freestream velocities, with the exception of around 40 ft/s, over the tuned cascade, and 1% and 2% mistuning. The 5% mistuning also compacts the damping values such that they are all equally damped.

For the most realistic analysis, random mistuning is investigated which is already apparent in compressor blades. The idea is to determine if the deviations already inherent in the real blades are beneficial or harmful to stability. The plunge stability is given in Fig. 3.18 and the pitch stability is given in Fig. 3.19. For plunge stability, the effect of random mistuning is harmful. All of the damping values are decreased indicating a more catastrophic flutter. Pitch stability only benefits from random mistuning at high freestream velocities, otherwise random mistuning is detrimental to pitch stability. Because random mistuning appears to be destructive, manufacturers should improve

upon their manufacturing tolerances and implement better wear resistance to their blades to reduce the amount of random mistuning.

Chapter 4: Concluding Remarks

4.1 Conclusions

This investigation was conducted to study the use of mistuning as a method for flutter control and cascade stabilization using a recently developed unsteady aerodynamic model applied to a compressor cascade. The following conclusions have been reached:

1) The recently developed single blade vortex lattice method finds excellent agreement with Theodorsen's, quasi-steady and quasi-static aerodynamic theories.

2) The vortex lattice method applied to a cascade finds good agreement with Whitehead's unsteady aerodynamics. The vortex lattice method solution moves towards Whitehead's unsteady aerodynamic theory solution as more blades are added to the cascade.

3) Unsteadiness introduces a reduction in lift and moment magnitude and creates a phase lag.

4) A single disturbed blade can be stabilized by giving its energy to the surrounding blades which in turn causes them to become slightly unstable.

5) When alternate mistuning is introduced, an exchange of energy occurs which causes particular blades to become stabilized and others to destabilize.

6) Mistuning, for case one, is not beneficial to flutter velocity. Mistuning quickly destabilizes the cascade and causes the blades to flutter. As the level of mistuning increases, the blades begin to diverge faster and more blades become excited and extract more energy.

7) Case two proves that mistuning has the potential to be used as a method of passive flutter control. The maximum benefit of mistuning for case two occurs around 1% and 5% mistuning.

8) Random mistuning is shown to be detrimental to pitch and plunge stability giving reason for manufacturers to improve their tolerances and wear resistance.

4.2 Recommendations for Future Research

Several recommendations for future work on this project have been made which are summarized as follows:

1) The vortex lattice model should be compared to a high fidelity computational fluid dynamics model for both a single blade and a cascade under high and low unsteadiness values to better determine the accuracy of the model rather than comparing it to other limited aerodynamic models.

2) The aeroelastic model needs to be verified against the results presented in the literature review along with both high fidelity models and experimental data found in more recent studies.

3) A final direction for this research would be to investigate high cycle fatigue, a leading cause of compressor failure. If the vortex lattice aerodynamic model was confirmed to be accurate, the model developed here would be useful in helping uncover the mechanisms that cause high cycle fatigue.

Tables

Table 2.1: Dormand-Prince method coefficients

0							
1/5	1/5						
3/10	3/40	9/40					
4/5	44/45	-56/15	32/9				
8/9	19372/6561	-25360/2187	64448/6561	-212/729			
1	9017/3168	-355/33	46732/5247	49/176	-5103/18656		
1	35/384	0	500/1113	125/192	-2187/6784	11/84	
	5179/57600	0	7571/16695	393/640	-92097/339200	187/2100	1/40
	35/384	0	500/1113	125/192	-2187/6784	11/84	0

Table 3.1: Blade and flow properties, case one

Property	**Value**	**Units**
B	12	
c	0.5	ft
x_a	0	
a	0	
ω_a	10	rad/s
ω_h	25	rad/s
ρ	.002378	slugs/ft^3
m	.1401	slugs
r_a	0.4082	ft
N	20	
M	80	
β	0.996	
M_∞	0.3	
sc	0.5	
θ	60	deg

Table 3.2: Blade and flow properties, case two

Property	**Value**	**Units**
B	20	
c	6	ft
x_a	0	
a	0	
ω_a	5	rad/s
ω_h	25	rad/s
ρ	.002378	slugs/ft^3
m	13.4411	slugs
r_a	0.5774	ft
N	20	
M	100	
β	0.996	
M_∞	0	
sc	1	
θ	60	deg

Table 3.3: Mistuning values for random mistuning

Blade	**Mistuning**
1	0.9877
2	0.9763
3	1.0531
4	1.0590
5	0.9374
6	0.9980
7	0.9891
8	1.0293
9	1.0419
10	1.0509
11	0.9552
12	1.0359
13	1.0310
14	0.9325
15	0.9238
16	0.9997
17	1.0919
18	0.9681
19	1.0171
20	0.9448

Figures

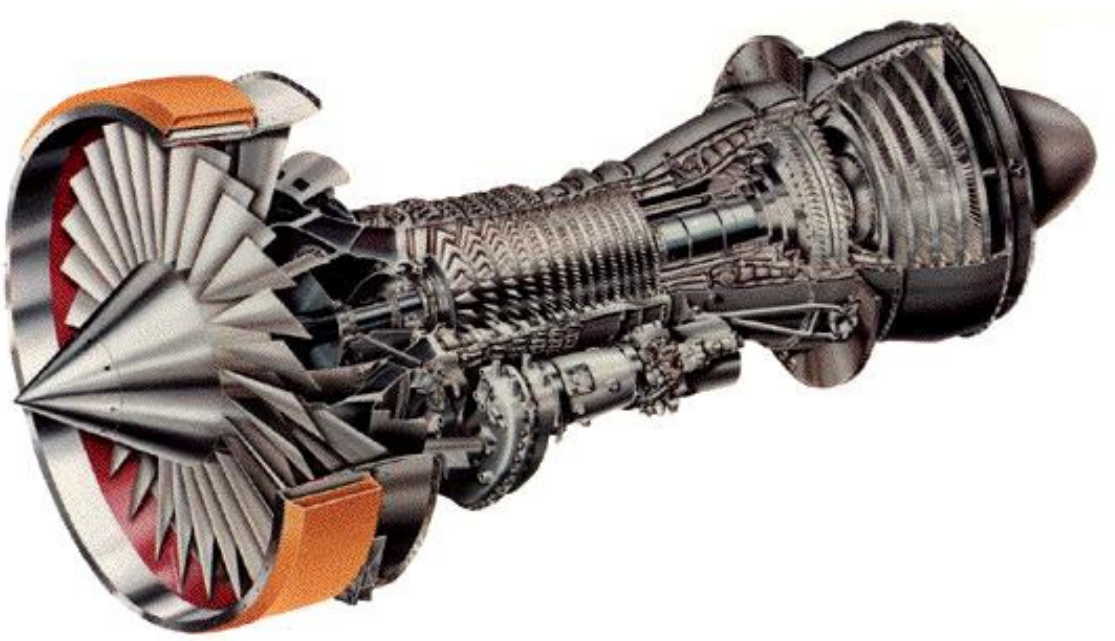

Figure 1.1: GE TF-34 turbofan engine [30]

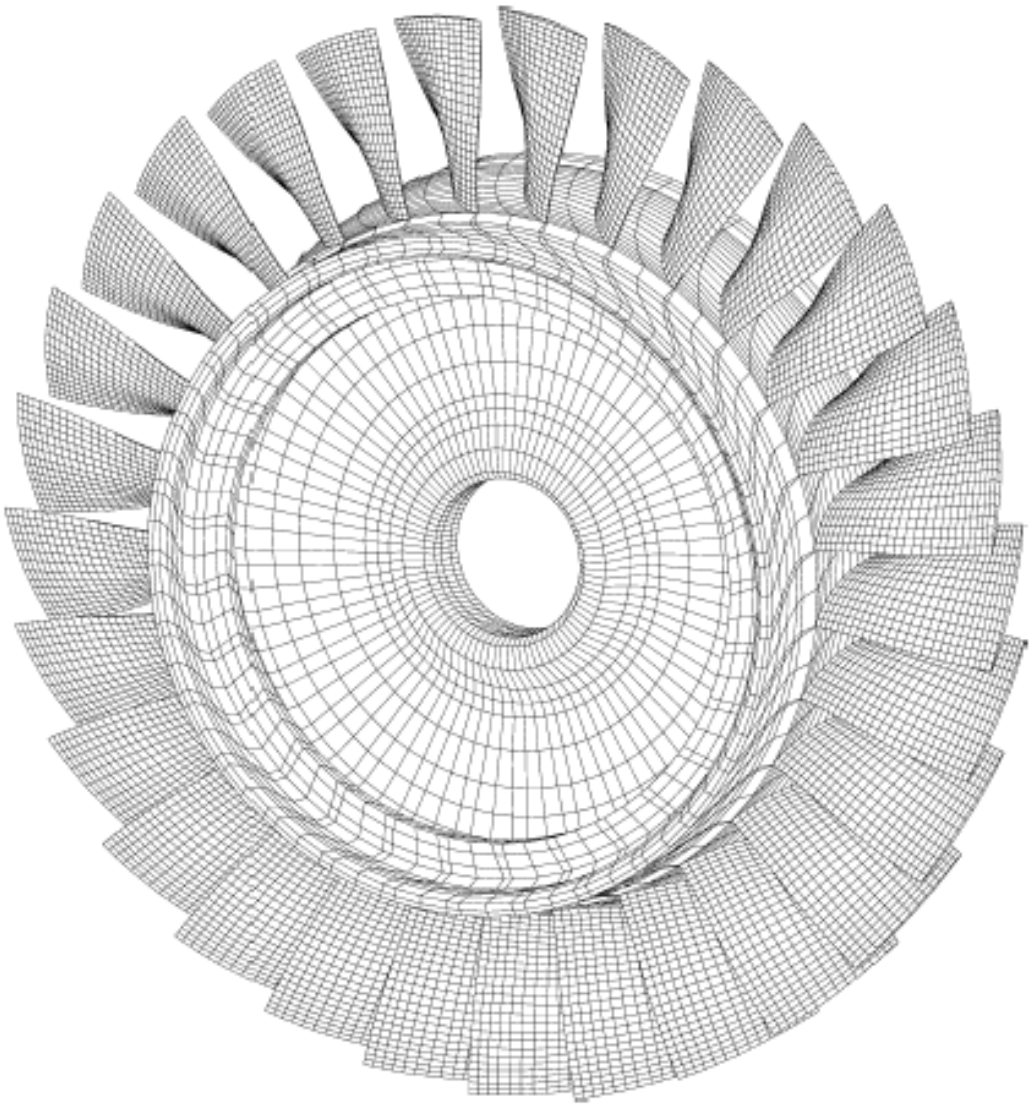

Figure 1.2: Computational model of a compressor rotor [31]

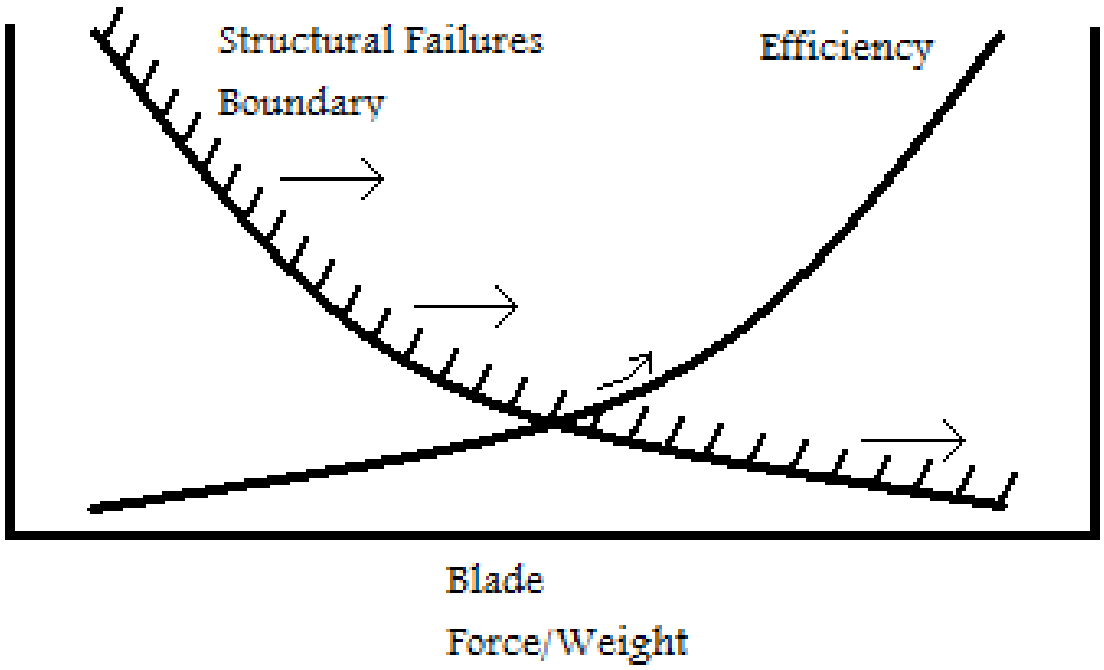

Figure 1.3: Relationship between efficiency and structural failures trends

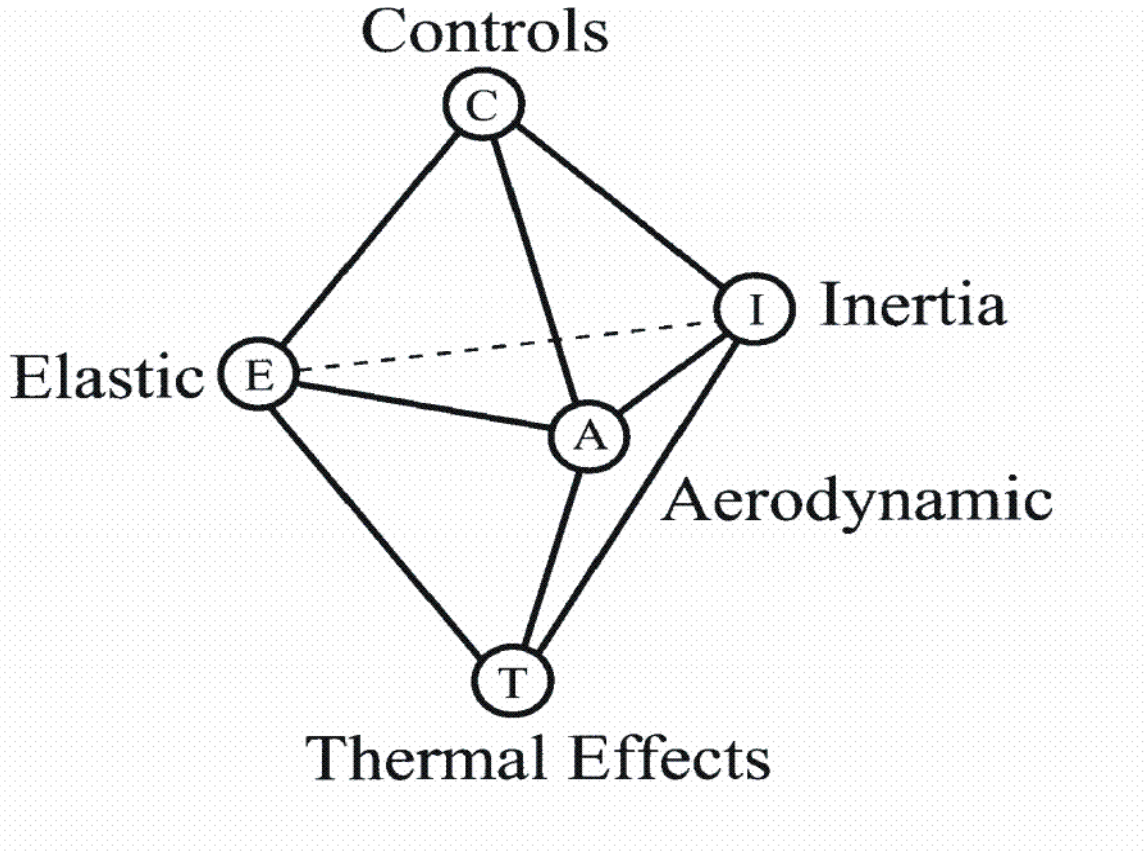

Figure 1.4: Collar's expanded triangle [32]

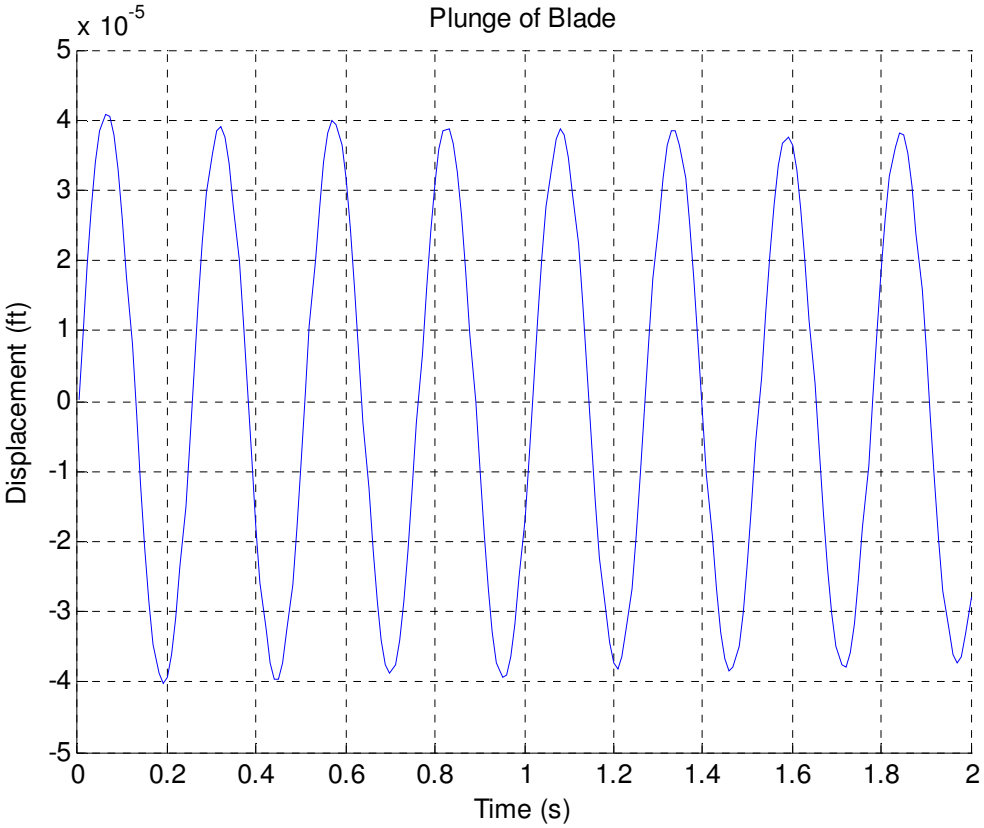

Figure 1.5: High cycle fatigue

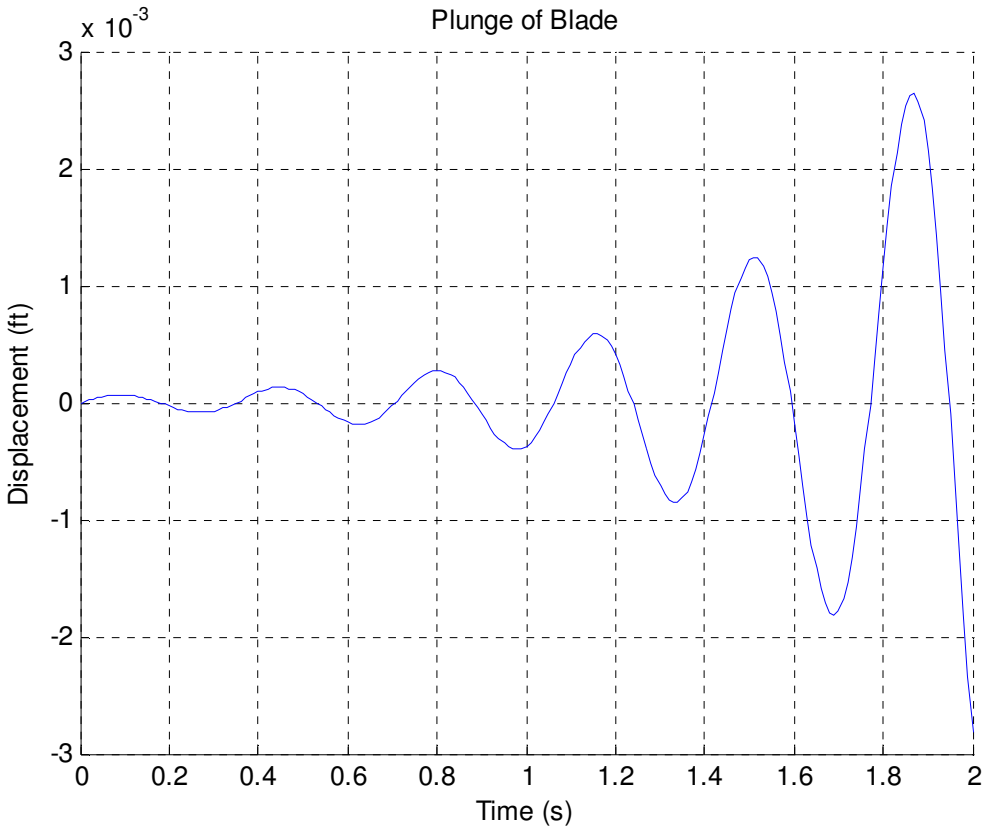

Figure 1.6: Flutter

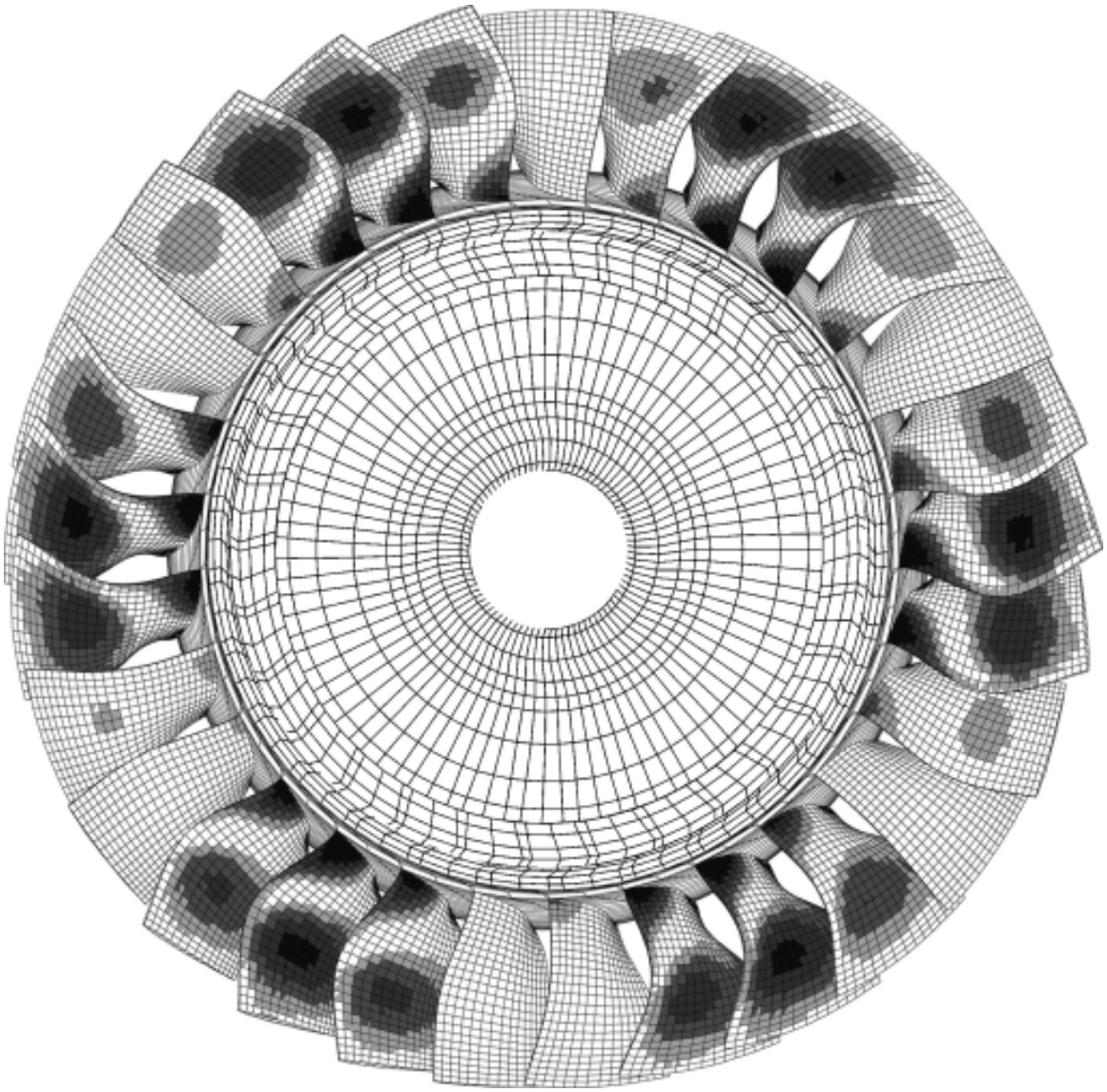

Figure 1.7: Tuned compressor rotor mode shapes [31]

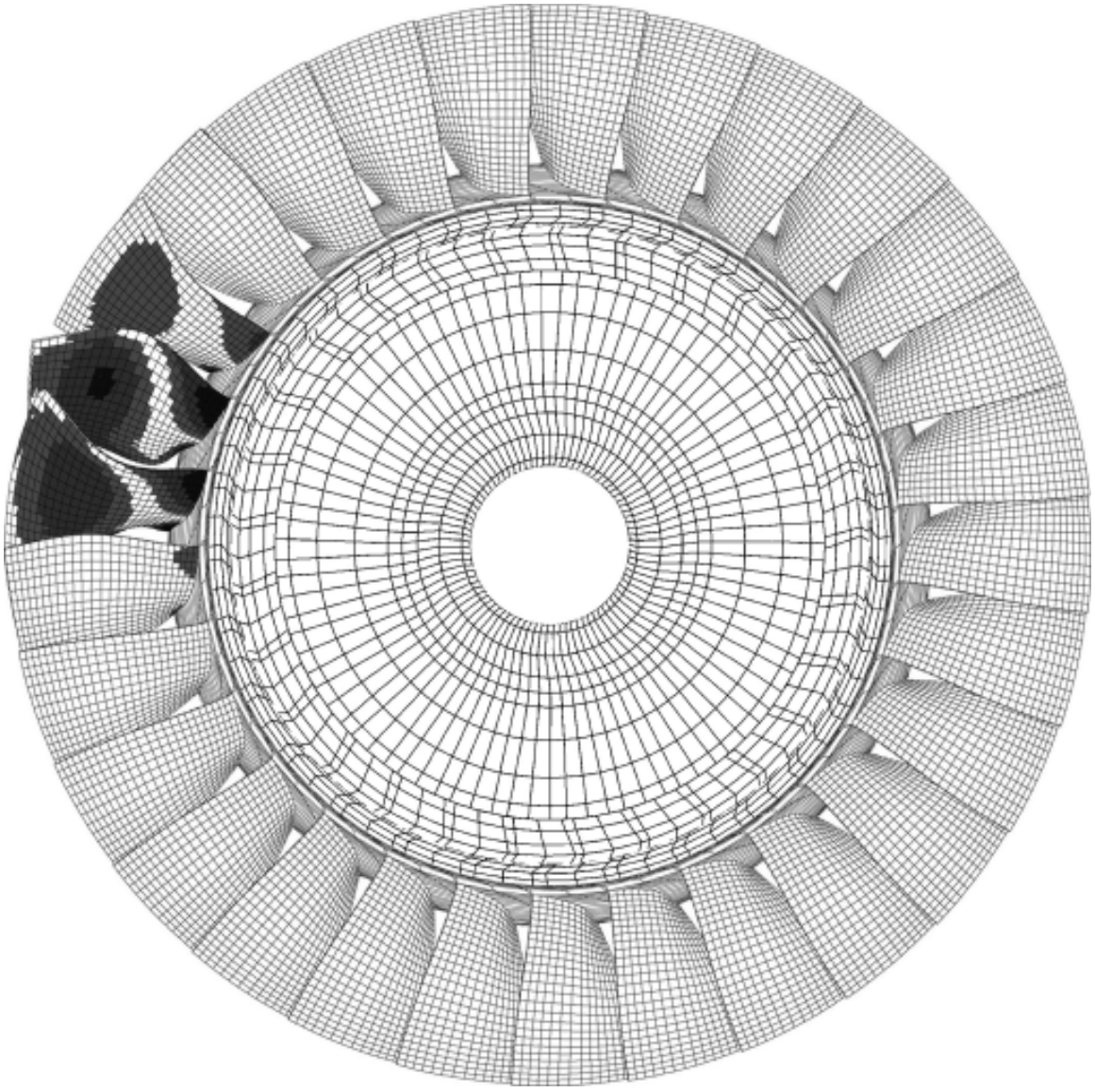

Figure 1.8: Mistuned compressor rotor mode shapes [31]

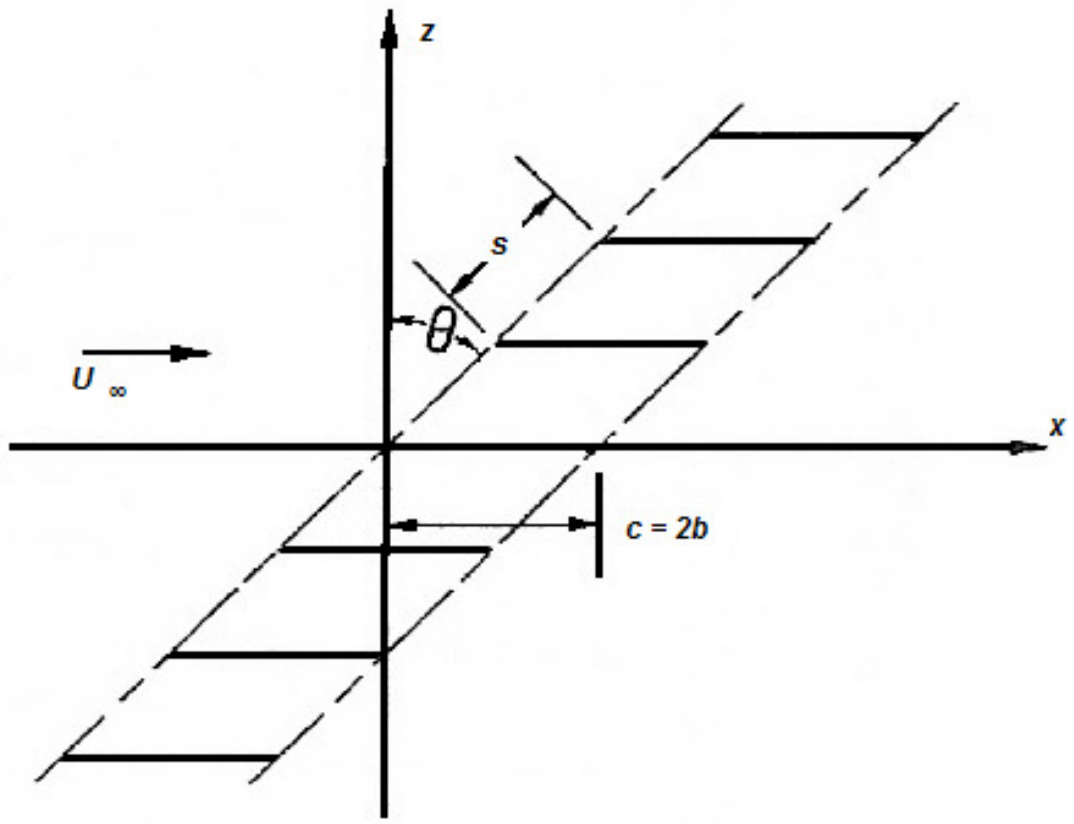

Figure 2.1: 2-D cascade geometry of compressor rotor [10]

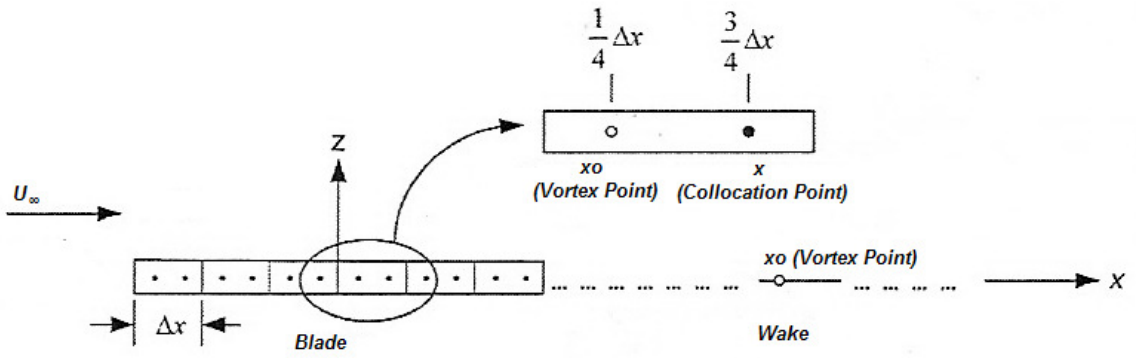

Figure 2.2: Vortex lattice/element model for a 2-D blade [22]

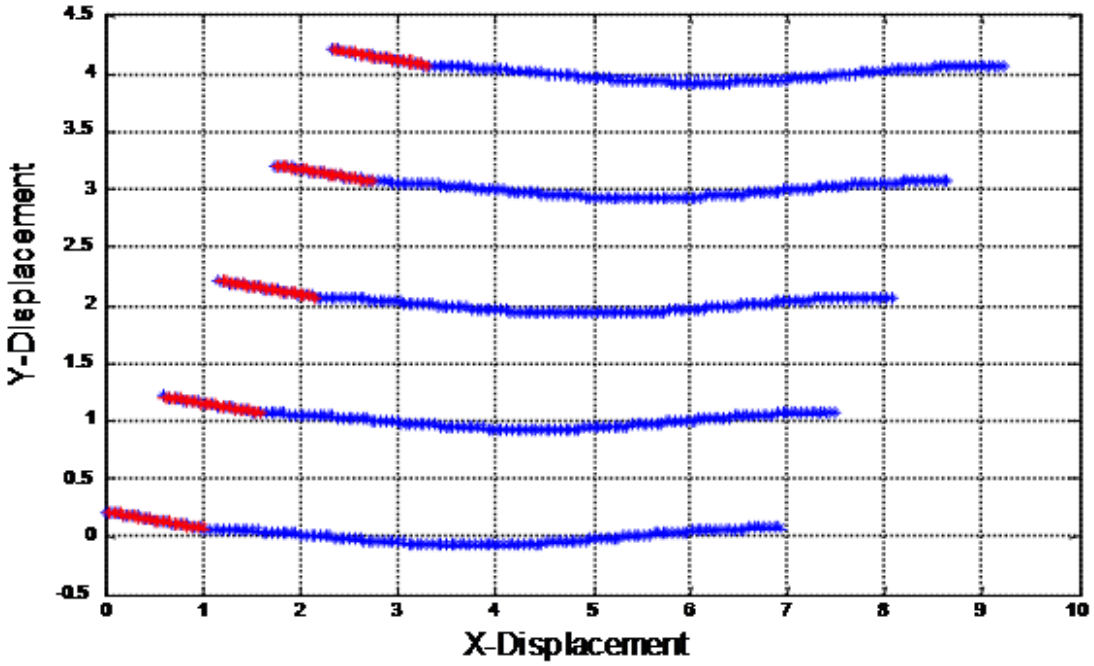

Figure 2.3: Motion of airfoil cascade with wake vortices

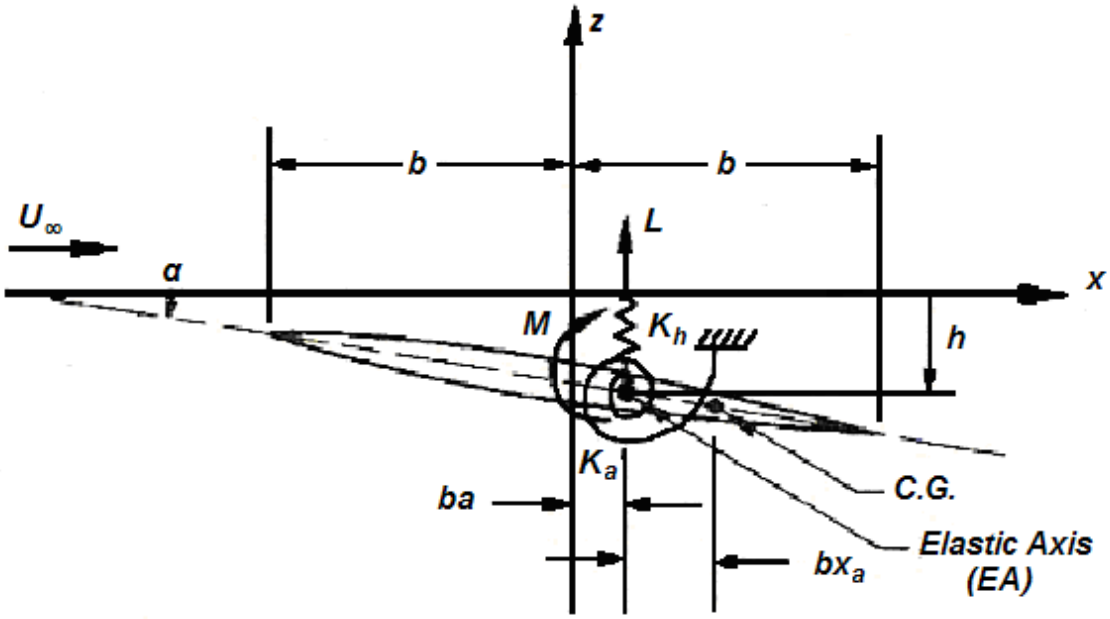

Figure 2.4: Blade geometry and structural model [10]

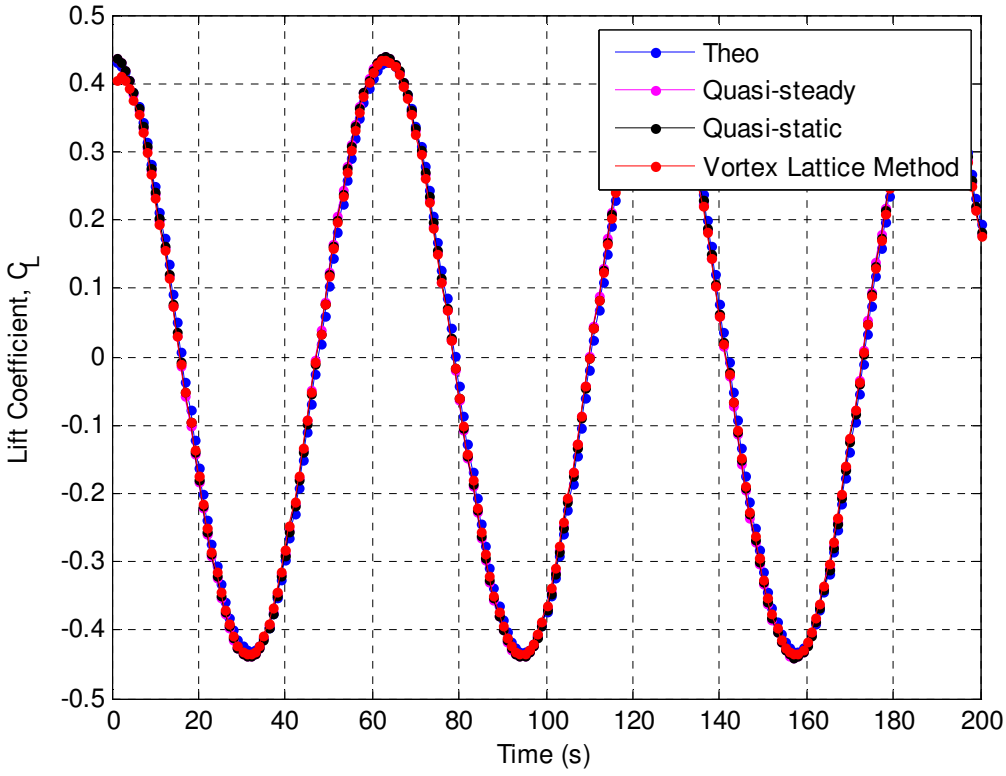

Figure 3.1: Lift comparison of single blade aerodynamic theories, k = 0.01

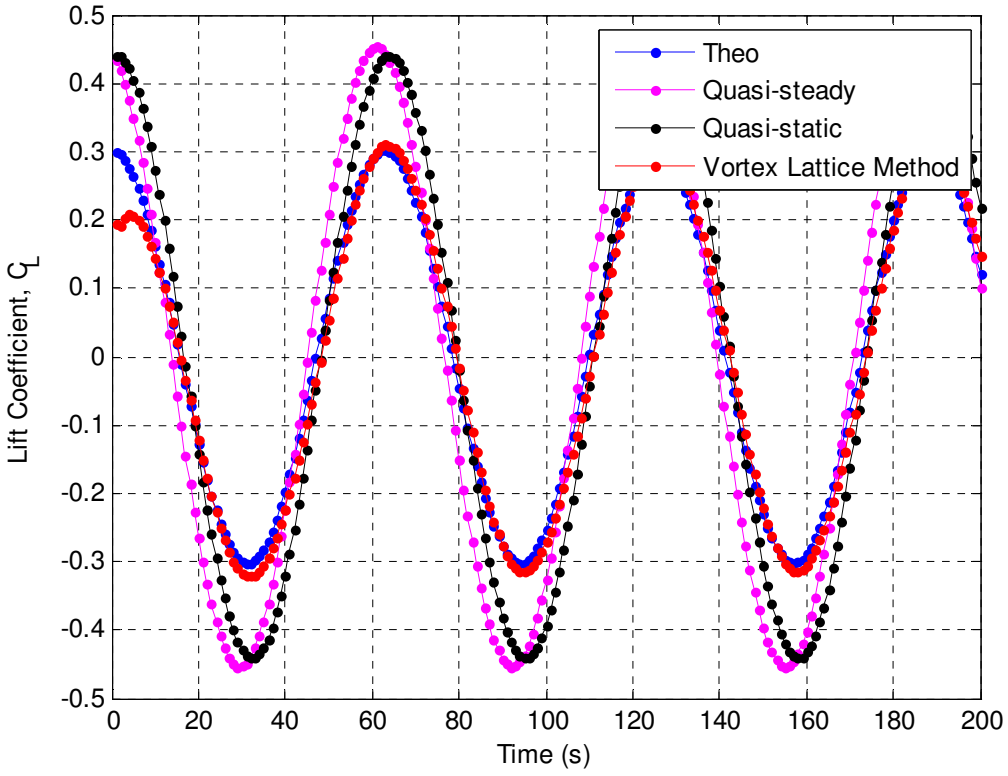

Figure 3.2: Lift comparison of single blade aerodynamic theories, k = 0.3

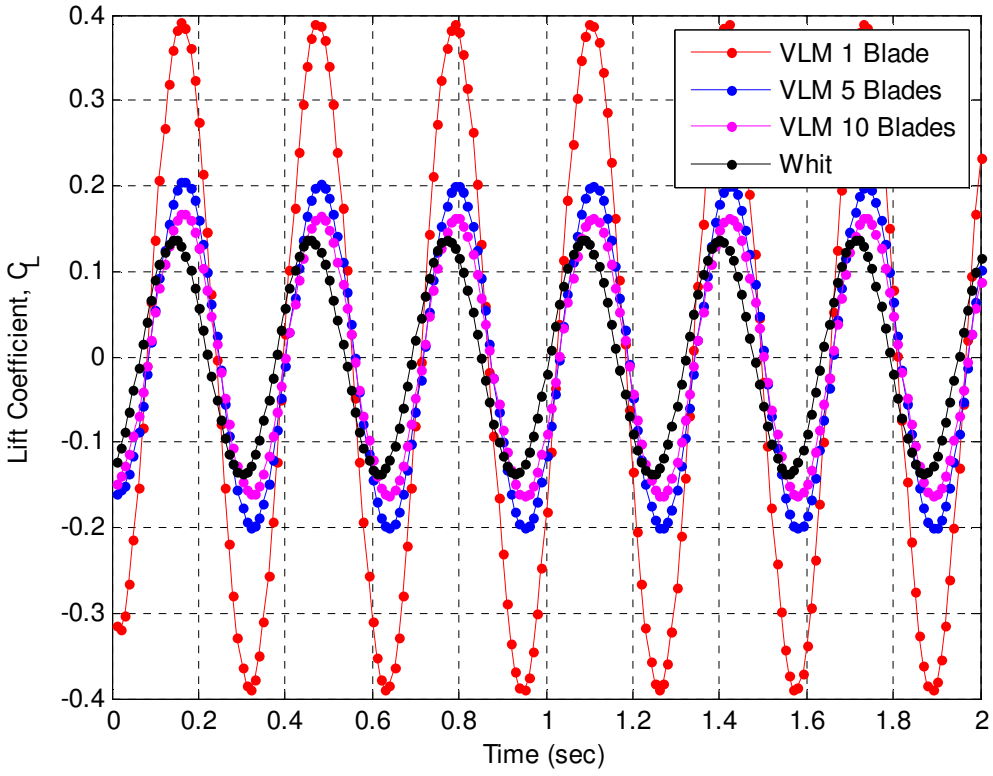

Figure 3.3: Lift comparison of cascade aerodynamic theories, k = 0.1

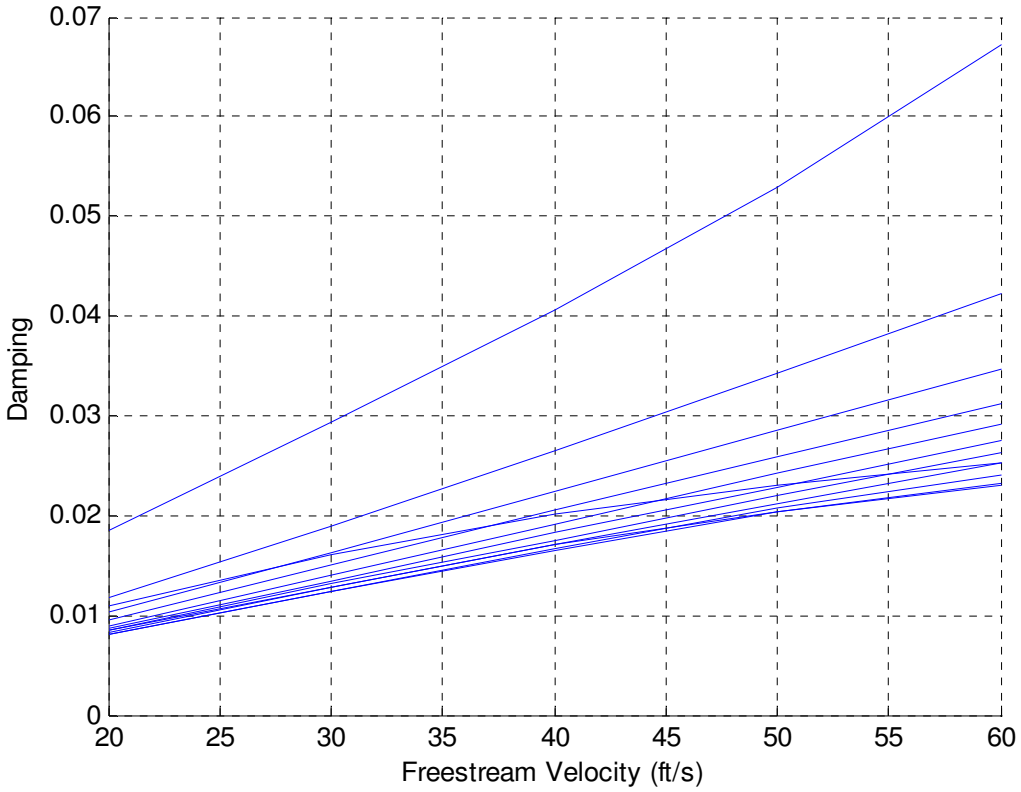

Figure 3.4: Plunge stability for case one, 0% mistuning

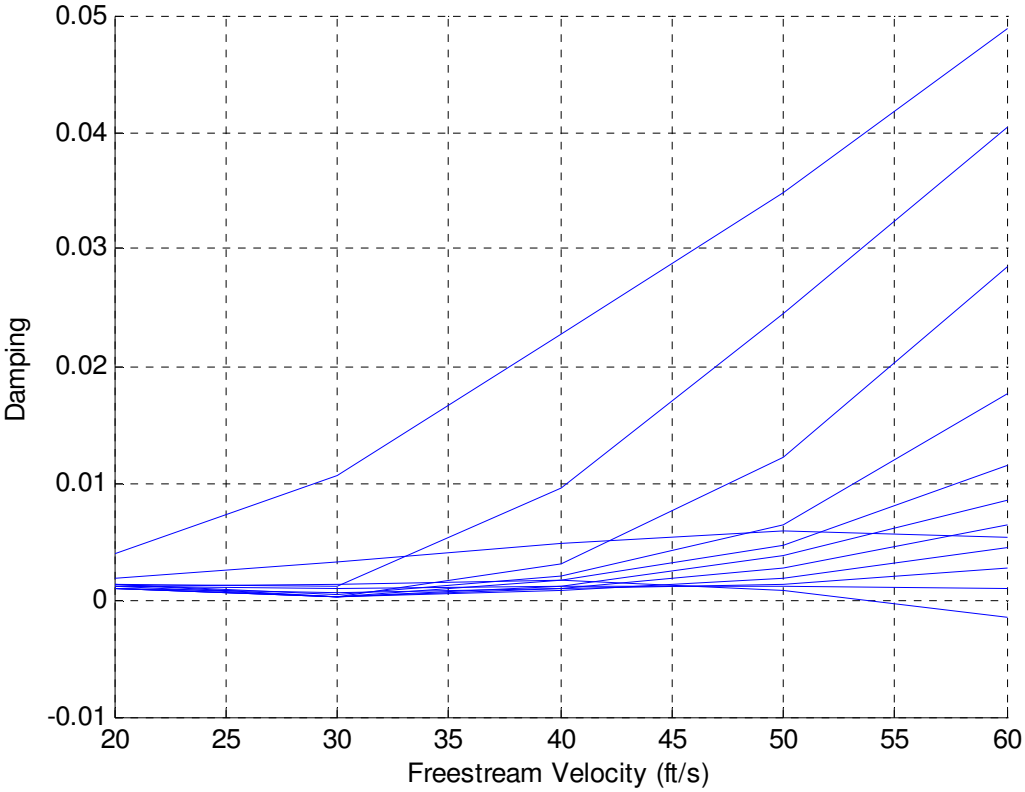

Figure 3.5: Pitch stability for case one, 0% mistuning

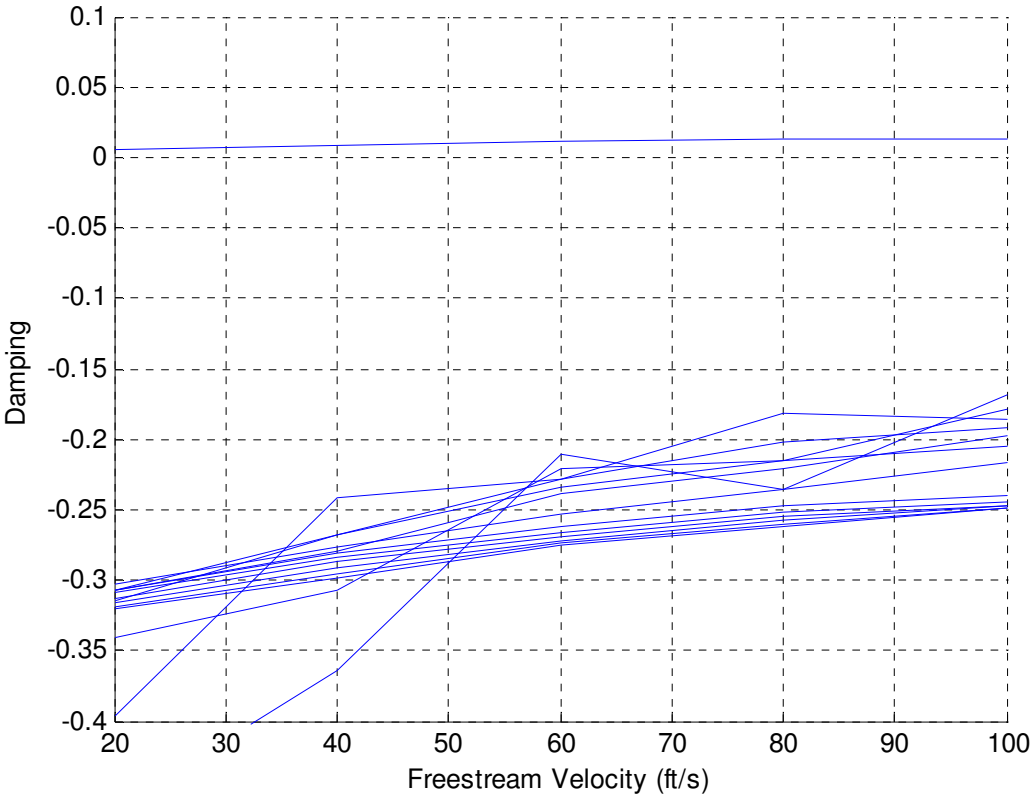

Figure 3.6: Plunge stability for case two, 0% mistuning

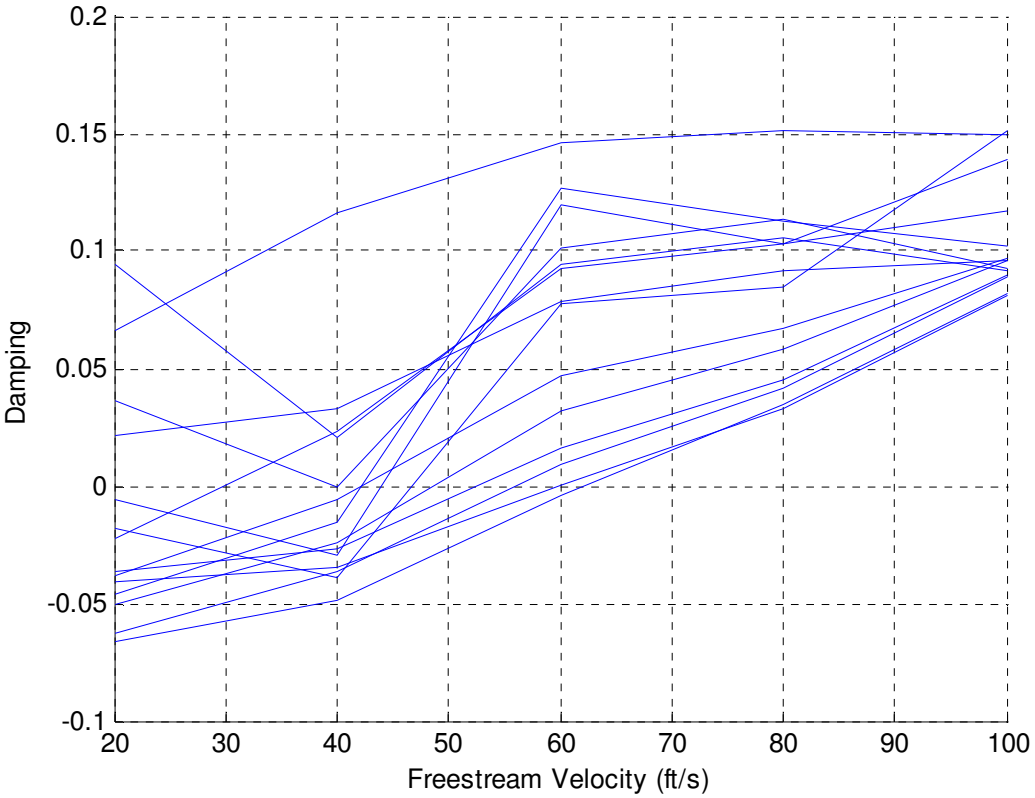

Figure 3.7: Pitch stability for case two, 0% mistuning

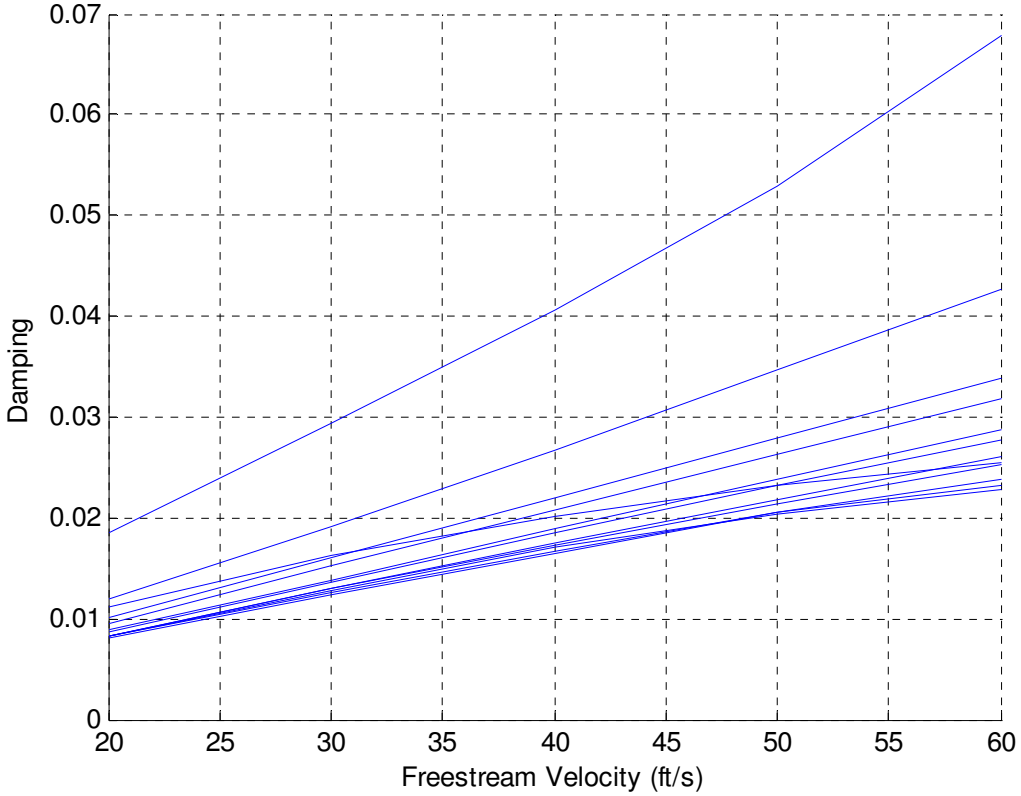

Figure 3.8: Plunge stability for case one, 1% mistuning

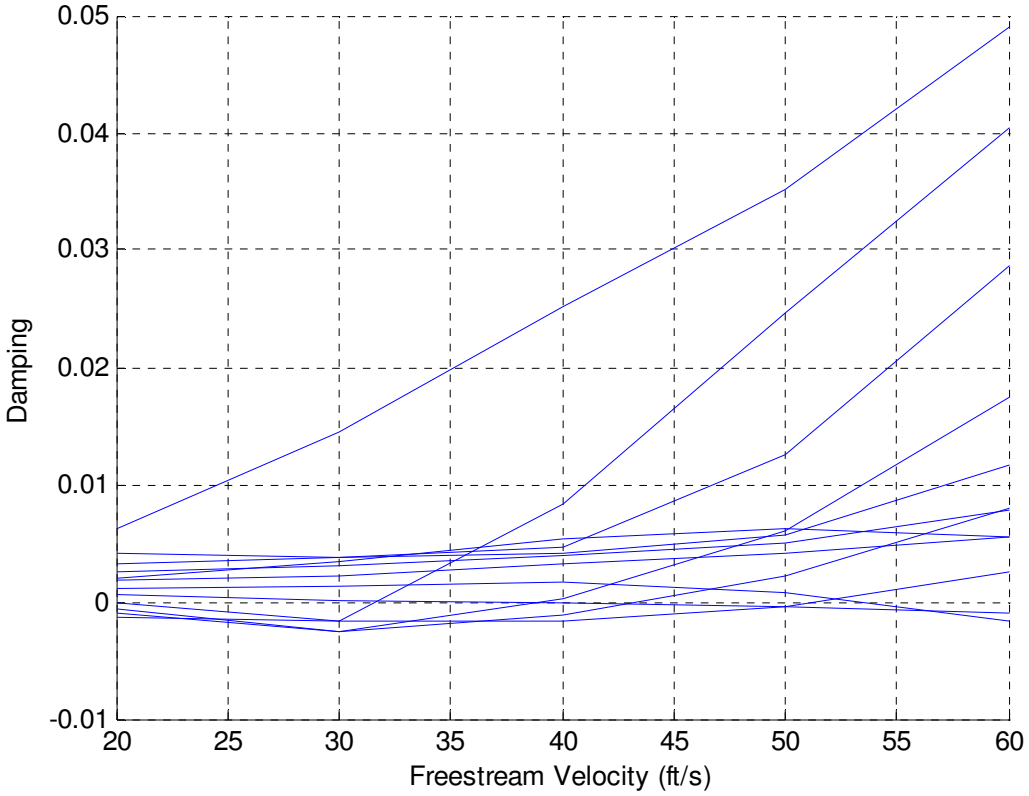

Figure 3.9: Pitch stability for case one, 1% mistuning

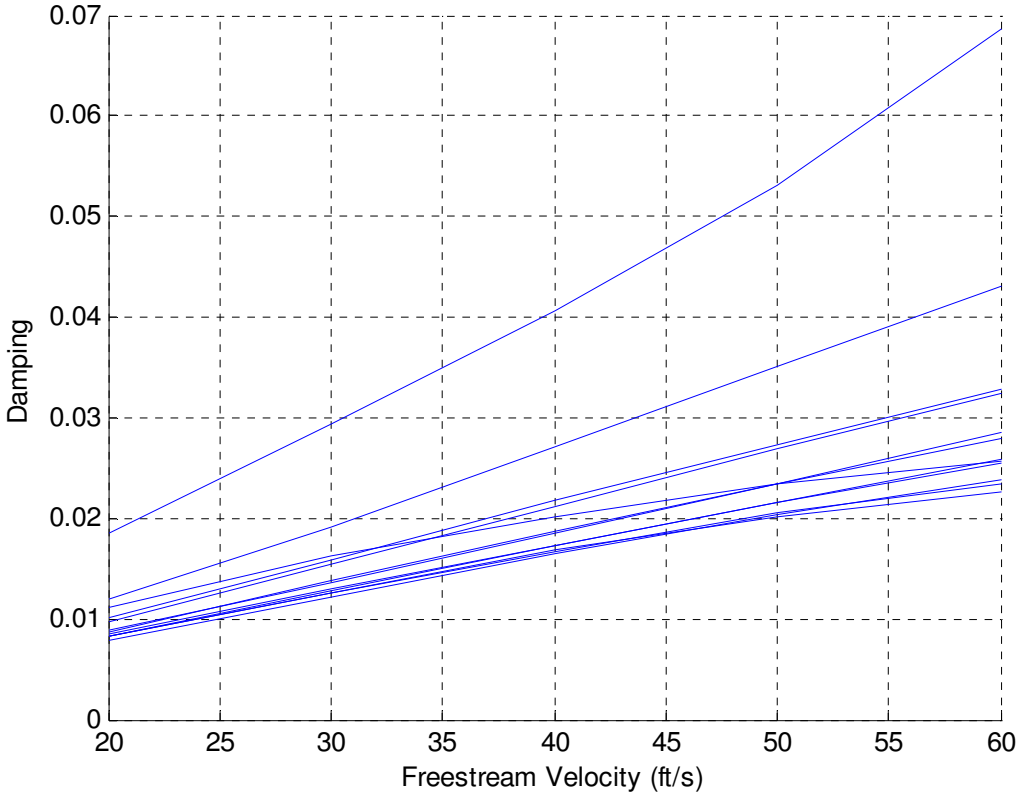

Figure 3.10: Plunge stability for case one, 2% mistuning

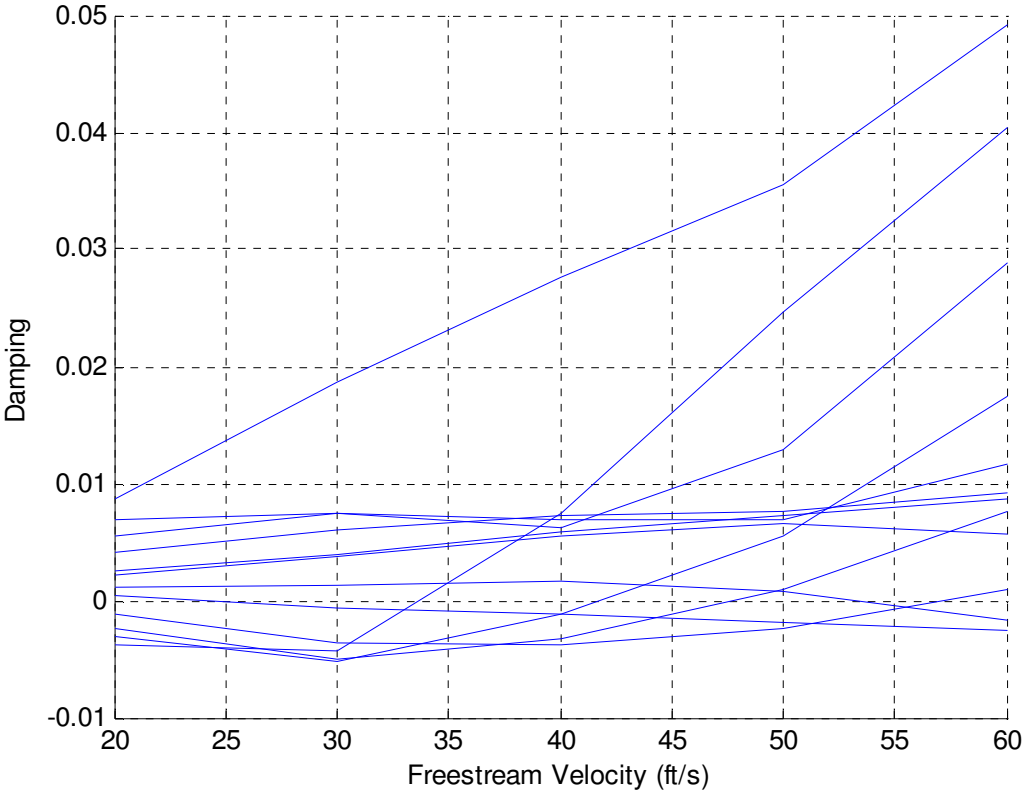

Figure 3.11: Pitch stability for case one, 2% mistuning

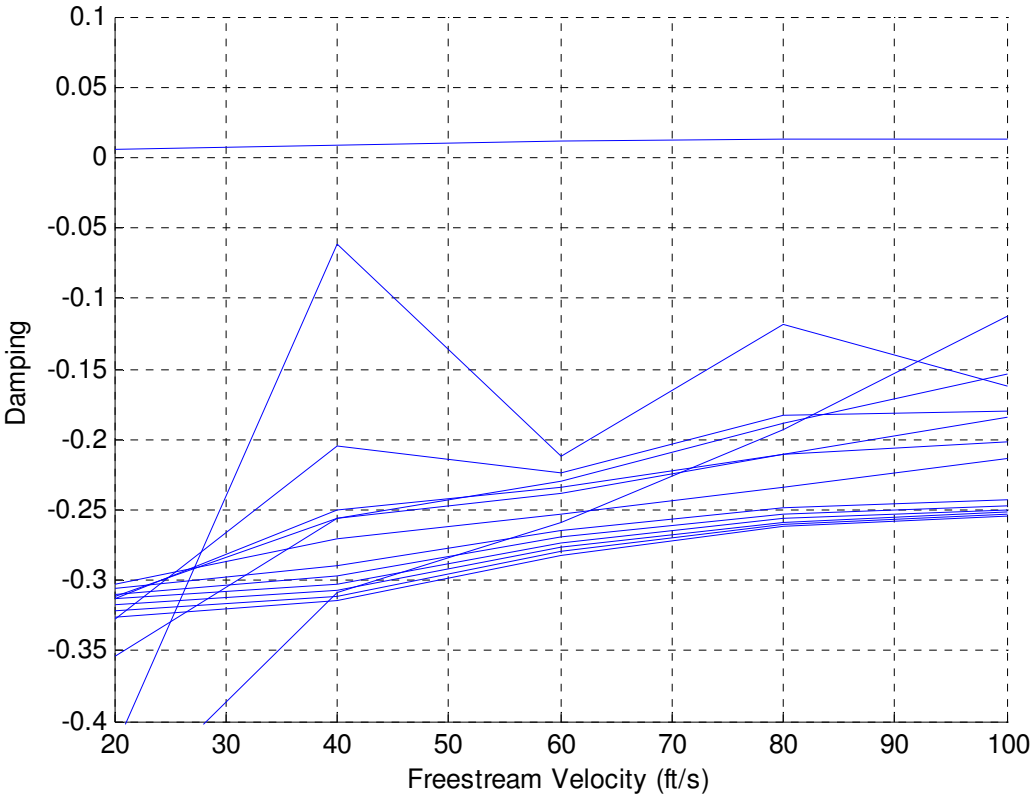

Figure 3.12: Plunge stability case two, 1% mistuning

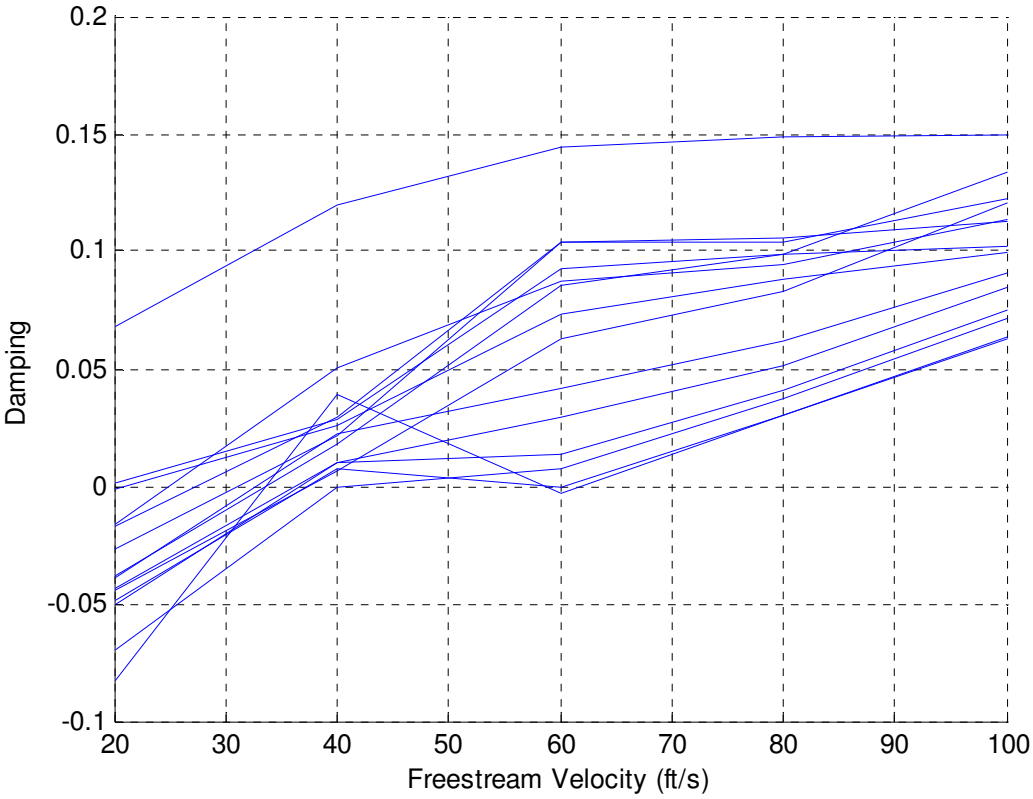

Figure 3.13: Pitch stability case two, 1% mistuning

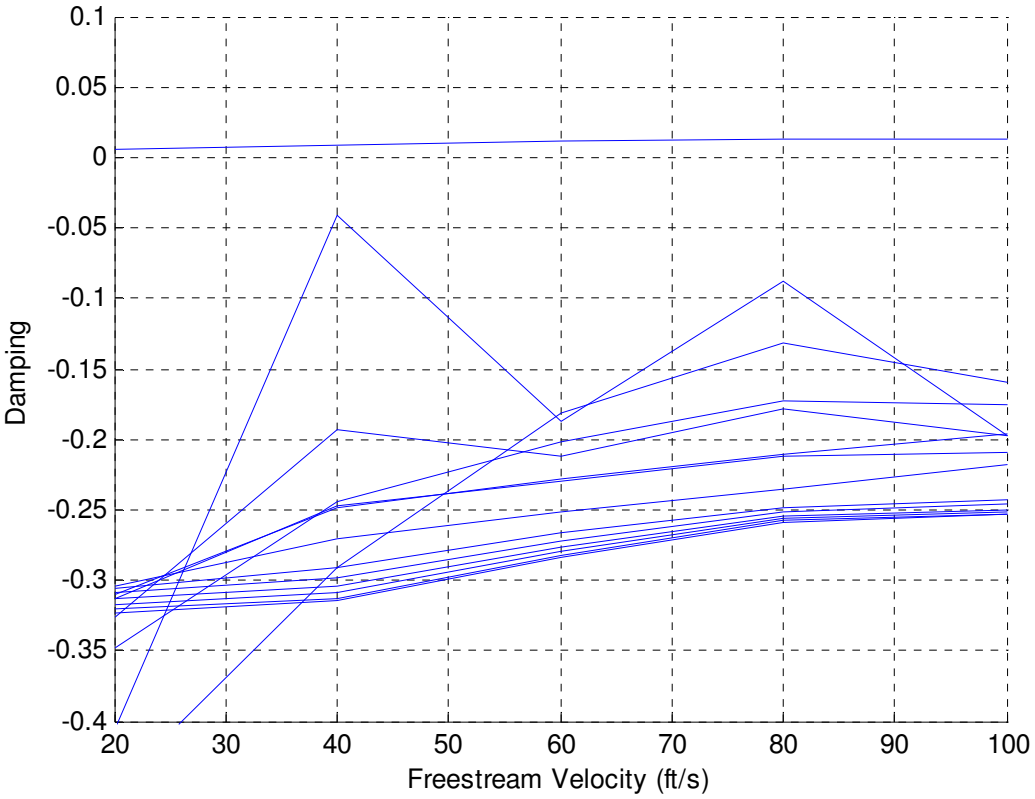

Figure 3.14: Plunge stability for case two, 2% mistuning

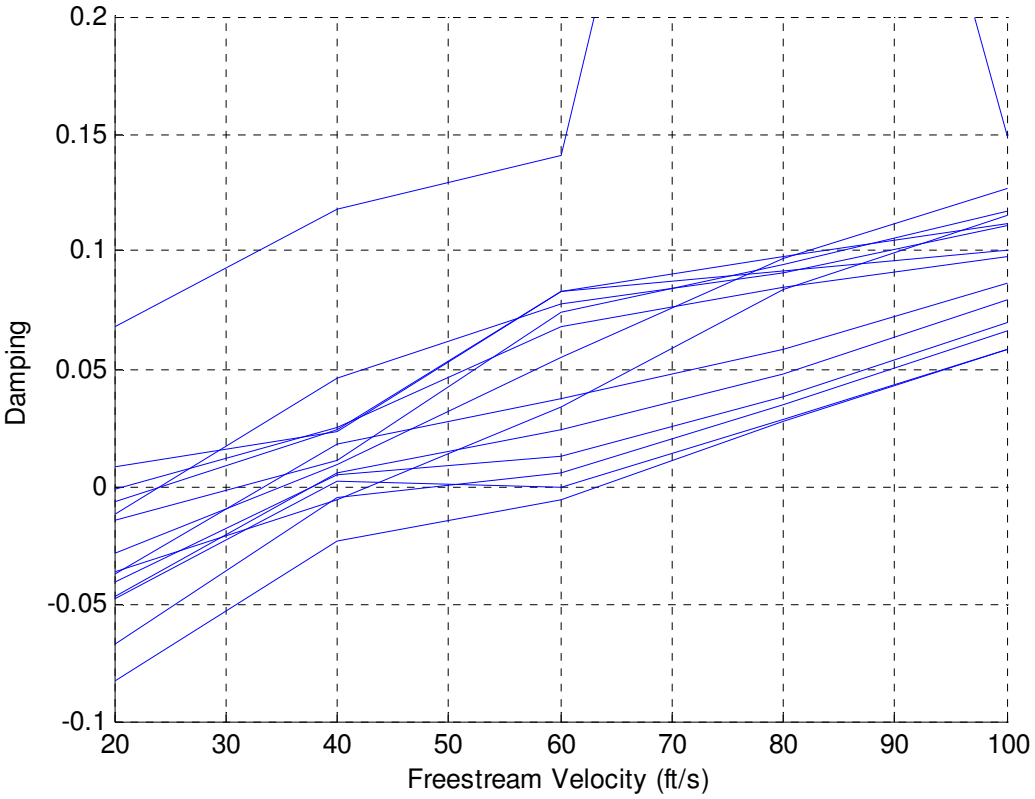

Figure 3.15: Pitch stability for case two, 2% mistuning

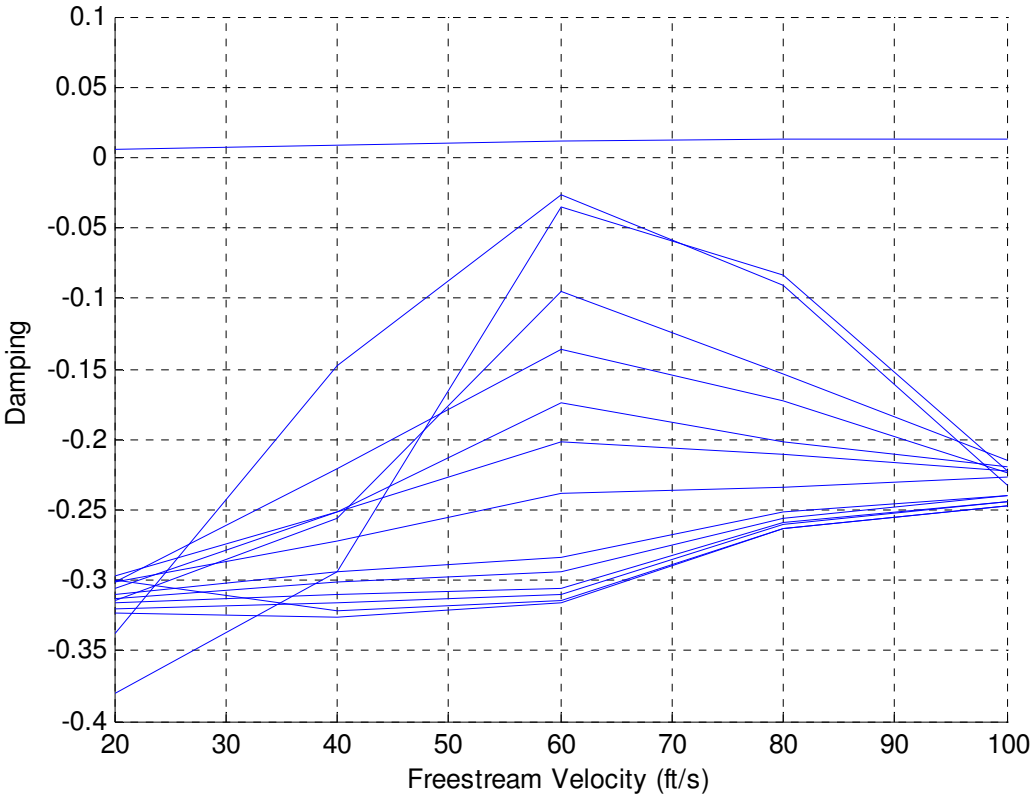

Figure 3.16: Plunge stability for case two, 5% mistuning

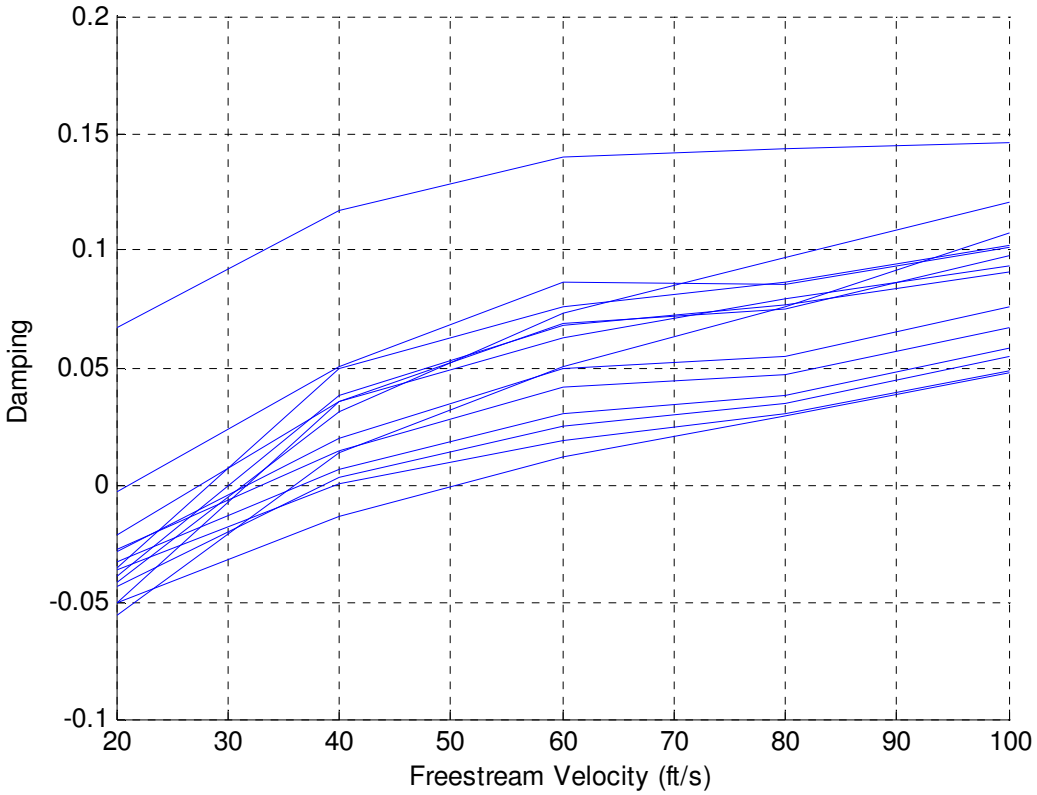

Figure 3.17: Pitch stability for case two, 5% mistuning

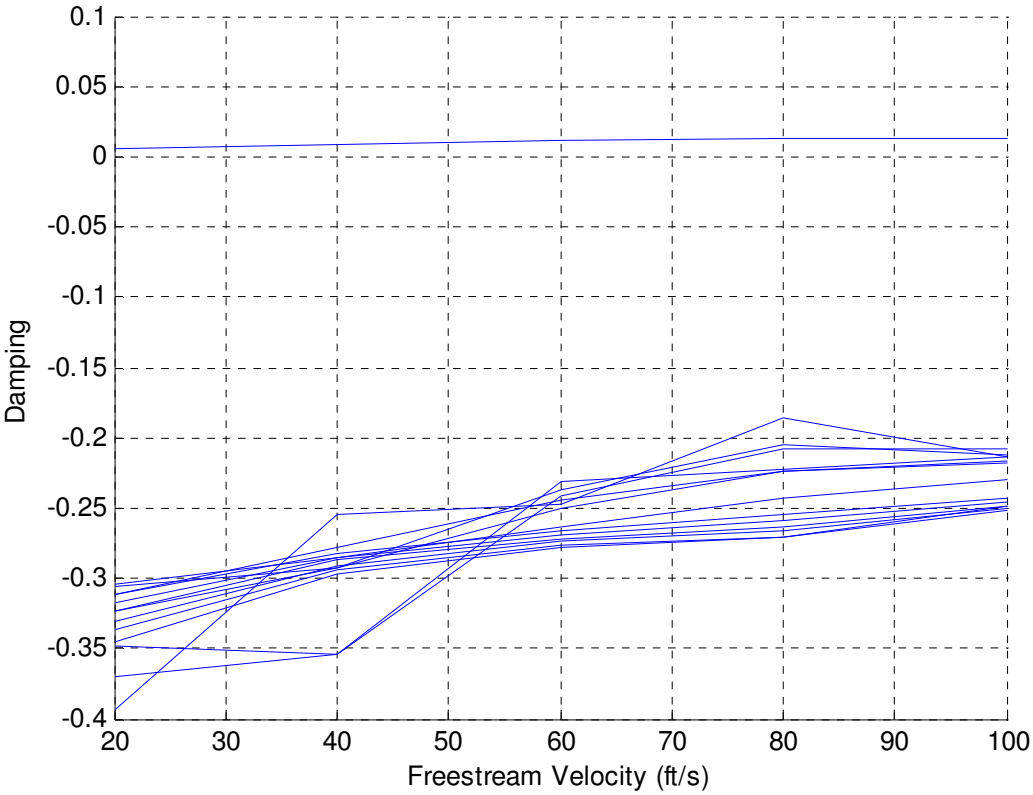

Figure 3.18: Plunge stability for case two, random mistuning

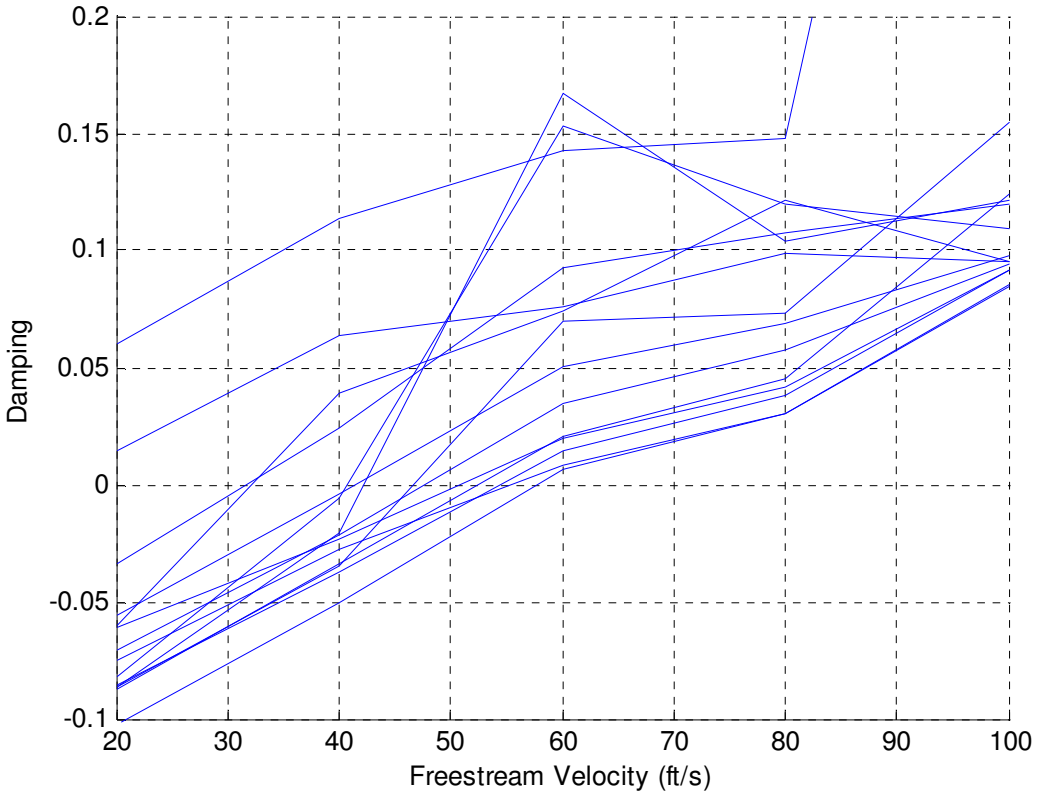

Figure 3.19: Pitch stability for case two, random mistuning

References

[1] Bendiksen, O. O., "Aeroelastic Problems in Turbomachinery," AIAA-90-1157.

[2] Hodges, D. H., and Pierce, G. A., *Introduction to Structural Dynamics and Aeroelasticity*, Cambridge Aerospace Series, New York, 2002.

[3] Shannon, J. F., "Vibration Problems in Gas Turbines, Centrifugal and Axial Flow Compressors," British A.R.C R&M 2226, 1945.

[4] Goatham, J. I., "Design Considerations for Large Fan Blades," SAE Paper 690387, April 1969.

[5] Jeffers, J. D., II, and Meece, C. E., Jr., "F100 Fan Stall Flutter Problem Review and Solution," *Journal of Aircraft*, 12, April 1975, 350-357.

[6] Mehmed, O., et al., "Bending-Torsion Flutter of a Highly Swept Advanced Turboprop," NASA TM-82975, 1982.

[7] Mikolajczak, A. A., et al., "Advances in Fan and Compressor Blade Flutter Analysis and Predicitons," *Journal of Aircraft*, 12, April 1975, 325-332.

[8] Troha, W., and Swain, K., "Composite Inlays Increase Flutter Resistance of Turbine Engine Fan Blades," ASME Paper 76-GT-29, The American Society of Mechanical Engineers, New York, New York, March 1976.

[9] Ware, T. C., Kobayashi, R. J., and Jackson, R. J., "High-Tip-Speed, Low-Loading Transonic Fan Stage," NASA CR-121263, 1974.

[10] Bendiksen, O., and Friedmann, P., "Coupled Bending-Torsion Flutter in Cascades," *AIAA Journal*, Vol. 18, No. 2, 1979.

[11] Whitehead, D. S., "Force and Moment Coefficients for Vibrating Aerofoils in Cascade," Great Britain A.R.C. R&M 3254, London, Feb. 1960.

[12] Cho, S. H., Kim, T., and Song, S. J., "A Time-Domain Fluid-Structure Interaction Analysis of Fan Blades," Proceedings of ASME Turbo Expo 2008, Berlin, Germany, June 2008.

[13] Movshovich, I. M., "Self-Induced Vibrations of Axial-Compressor Blades," *Transactions of the Moscow Aviation Institute*, No. 172, Moscow, 1967. Translated in NASA TT F-547, "Investigation of Vibration and Stability of Aircraft Components," edited by G. S. Skubackevskiy, Washington, D.C., 1969, pp. 71-82.

[14] Dye, R. C. F., and Henry, T. A., "Vibration Amplitudes of Compressor Blades Resulting from Scatter in Blade Natural Frequencies," *Journal of Engineering for Power*, Vol. 91, No. 3, 1969, pp. 182-188.

[15] Ewins, D. J., "The Effect of Detuning upon the Forced Vibration of Bladed Disks," *Journal of Sound and Vibration*, Vol. 9, No. 1, 1969, pp. 65-79.

[16] Ewins, D. J., "Vibration Modes of Mistuned Bladed Disks," *Journal of Engineering for Power*, Vol. 98, No. 3, 1976, pp.349-355.

[17] Whitehead, D. S., "Torsional Flutter of Unstalled Cascade Blades at Zero Deflection," Great Britain A.R.C. R&M 3429, 1964.

[18] Whitehead, D. S., "Bending Flutter of Unstalled Cascade Blades at Finite Deflection," Great Britain A.R.C. R&M 3386, 1962.

[19] Whitehead, D. S., "Effect of Mistuning of Vibration of Turbo-Machine Blades Induced by Wakes," *Journal of Mechanical Engineering Science*, Vol. 8, No. 1, 1966, pp. 15-21.

[20] Kaza, K. R. V., and Kielb, R. E., "Effects of Mistuning on Bending-Torsion Flutter and Response of a Cascade in Incompressible Flow," 1981.

[21] Sadeghi, M., and Liu, F., "Investigation of Mistuning Effects on Cascade Flutter Using a Coupled Method," *Journal of Propulsion and Power*, Vol. 23, No. 2, 2007, pp. 266-272.

[22] Cho, S. H., Kim, T., Song, S. J., and Shin, S. J., "Aeroelastic Analysis of an Isolated Airfoil Under a Pulsating Flow," *AIAA Journal*, Vol. 45, No. 5, May 2007.

[23] Katz, J., and Plotkin, A., *Low-Speed Aerodynamics*, 2nd ed., Cambridge Univ. Press, Cambridge, England, U.K., 2001.

[24] Hall, K. C., "Eigenanalysis of Unsteady Flows about Airfoils, Cascades, and Wings," *AIAA Journal*, Vol. 32, No. 12, 1994, pp. 2426-2432.

[25] Kim, T. H., Nam, C. H., and Kim, Y. D., "Reduced-Order Aeroservoelastic Model with an Unsteady Aerodynamic Eigenformulation," *AIAA Journal*, Vol. 35, No. 6, 1997, pp. 1087, 1088.

[26] Anderson, J. D., *Fundamentals of Aerodynamics*, 4th ed., McGraw-Hill Companies, Inc., New York, 2007, pp. 668-672.

[27] Bisplinghoff, R. L., Ashley, H., and Halfman, R. L., *Aeroelasticity*, Dover Publications, Inc., New York, 1996.

[28] Dormand, J. R. and P. J. Prince, "A family of embedded Runge-Kutta formulae," *J. Comp. Appl. Math.*, Vol. 6, 1980, pp 19-26.

[29] McNamara, J. J., and Friedmann, P. P., "Flutter-Boundary Identification for Time-Domain Computational Aeroelasticity," *AIAA Journal*, Vol. 45, No. 7, Jul. 2007, pp. 1546-1555.

[30] "GE TF-34 Cutaway," *epower-propulsion.com*, iCentral LLC, <http://www.epower-propulsion.com/epower/gallery/ABP-GE%20TF34%20cutaway.htm>

[31] Castanier, M. P., and Pierre, C., "Modeling and Analysis of Mistuned Bladed Disk Vibration: Status and Emerging Directions," *Journal of Propulsion and Power*, Vol. 22, No. 2, Apr. 2006, pp. 384-396.

[32] Friedmann, P. P., "Renaissance of Aeroelasticity and its Future," *Journal of Aircraft,* Vol. 36, No. 1, Jan.-Feb. 1999, pp.105-121.